

THESIS

CHARACTERIZING 30-YEARS OF CONIFER REGENERATION PATTERNS IN HIGH-SEVERITY
WILDFIRES: A SNOW-COVER REMOTE SENSING APPROACH

Submitted by

Casey Menick

Department of Forest and Rangeland Stewardship

In partial fulfillment of the requirements

For the Degree of Master of Science

Colorado State University

Fort Collins, Colorado

Summer 2023

Master's Committee:

Advisor: Chad M. Hoffman

Co-Advisor: Wade T. Tinkham

Melanie K. Vanderhoof

Jody C. Vogeler

Copyright by Casey Menick 2023

All Rights Reserved

ABSTRACT

CHARACTERIZING 30-YEARS OF CONIFER REGENERATION PATTERNS IN HIGH-SEVERITY WILDFIRES: A SNOW-COVER REMOTE SENSING APPROACH

The number of large, high-severity wildfires has been increasing across the Western United States. It is not fully understood how wildfire intensification may impact conifer forests of the West, whose resilience is dependent on successful seedling regeneration. It is important to understand how conifer-dominated forests are able to recolonize high-severity burn patches and subsequently respond to shifting disturbance regimes. The goal of our research is to characterize patterns of conifer recolonization within high-severity burn patches over a 30-year study period. We investigate 34 high-severity wildfire complexes that occurred between 1988 and 1991 in conifer-dominated ecosystems of the northern Rocky Mountains. Composite snow-cover Landsat imagery was utilized to isolate conifer-specific vegetation by diminishing spectral contributions from soil and deciduous vegetation. Conifer regeneration was determined to be detectable by Landsat 11-19 years post-fire across forest types and at >10% canopy cover using snow-cover imagery. The trajectory of snow-cover Landsat NDVI was utilized to project future recovery time to pre-fire conifer vegetation levels for lodgepole pine (29.5 years), Douglas-fir (36.9 years), and fir-spruce forests (48.7 years). The presence of conifer regeneration was then modeled at 3-year intervals post-fire to characterize the progression of recolonization. Conifer recolonization analysis showed that 65% of the total high-severity burn area was reforested after

30 years. Across all high-severity patches, median patch recolonization was 100% within lodgepole pine, 91.1% within Douglas-fir, and 41.3% within fir-spruce. Patch fragmentation occurred across all size classes and forest types, with the majority of the remaining unforested area in Douglas fir (76%), lodgepole pine (61%), and fir-spruce (50%) transitioning to smaller unforested patch size classes. While we identified overall patterns of conifer resilience, high-severity burn patches with lower likelihoods of 30-year conifer recovery had lower edge-densities, drier climates, steeper slopes, higher elevations, and fir-spruce forests. These findings have implications for climate change resilience and may be applied to support forest restoration decision-making following high-severity wildfire. Future analyses should be conducted using snow-cover remote sensing imagery to identify patterns of post-disturbance conifer recovery over a wider spatial and temporal extent.

ACKNOWLEDGEMENTS

I am incredibly grateful to the many people who have supported me through my academic journey. My advisor, Wade Tinkham, for his constant encouragement, guidance, and above-and-beyond support throughout my time at CSU. My advisor, Chad Hoffman, for providing perceptive feedback, clear direction, and willingness to take on additional responsibilities. I am also grateful to my committee members, Melanie Vanderhoof and Jody Vogeler, for their wonderful insight, expertise, and encouragement of my research. I would like to thank my fellow lab members, NASA DEVELOP team, and FRS graduate students for their support and inspiration. I am thankful for my partner, friends, and family for their love and support throughout my academic career.

TABLE OF CONTENTS

ABSTRACT	ii
ACKNOWLEDGEMENTS	iv
LIST OF TABLES.....	vii
LIST OF FIGURES.....	viii
CHAPTER 1: CHARACTERIZING 30-YEARS OF CONIFER REGENERATION PATTERNS IN HIGH-SEVERITY WILDFIRES: A SNOW-COVER REMOTE SENSING APPROACH.....	1
1.1 Introduction	1
1.2 Methods	6
1.2.1 Study Area.....	6
1.2.2 Fire Selection	9
1.2.3 Identification of High-Severity Burn Patches.....	10
1.2.4 Snow-cover Landsat Imagery.....	12
1.2.5 Modelling Snow-Cover dNDVI Trajectory	13
1.2.6 Modelling Conifer Presence and Absence.....	14
1.2.7 Landscape and Patch-level Recolonization	16
1.2.8 Spatial Patterns of Recolonization	16
1.2.9 Identifying Characteristics of Recovery.....	18
1.3 Results	19
1.3.1 High-severity Burn Patch Distribution.....	19
1.3.2 Snow-Cover dNDVI Recovery and Detection.....	20
1.3.3 Conifer Presence-Absence Model Performance.....	21
1.3.4 Patch Fragmentation and Conifer Recolonization	22
1.3.5 Evaluation of Patch Recovery	26
1.4 Discussion	28
1.4.1 Trends of Snow-cover dNDVI Recovery	28

1.4.2 Evaluating Snow-cover Landsat Detectability	30
1.4.3 Patterns of Conifer Recolonization	32
1.4.4 Characteristics of Recovered Patches and Implications for Resilience.....	35
1.4.5 Limitations and Future Directions.....	36
1.5 Conclusion	38
Cited Works	40
Appendices	60

LIST OF TABLES

Chapter 1:	Characterizing 30-years of conifer regeneration patterns in high-severity wildfires: a snow-cover remote sensing approach	
Table 1.1.	Distribution of the number and area of high-severity burn patches evaluated within the study area. Patches are arranged by forest type groups Douglas-fir, fir-spruce, and lodgepole pine and by patch size class.....	20
Table 1.2.	Conifer presence-absence Random Forest model error matrix from independent validation expressed in terms of proportion of total area represented by each class. Total (W_i) represents the mapped area proportions and U_i characterizes the user's accuracy of each class	22
Table 1.3.	Odds-ratios from the generalized linear logistic regression model of conifer recovery. Odds-ratios greater than one indicate an increased likelihood of reaching 80% recovery 30 years post-fire, where values less than one indicate a reduced likelihood of recovery. Continuous predictors show the odds-ratio as the change in recovery likelihood for a one unit increase of that predictor. The interquartile range (IQR) odds-ratio shows the change in odds of conifer recovery across the interquartile range of that variable to provide more relevant comparisons between predictors across the study area. Categorical predictors show the relative difference in odds between each pairwise comparison, with the same odds reported for both ratios.....	27

LIST OF FIGURES

Chapter 1:	Characterizing 30-years of conifer regeneration patterns in high-severity wildfires: a snow-cover remote sensing approach	
Figure 1.1.	Study area map of the 34 high-severity fire events used in our analysis, with fire extents highlighted in black. The dashed boundary line indicates the combined area of the US portion of the EPA Level-III Ecoregion groups Canadian Rockies, Northern Rockies, Middle Rockies, and Idaho Batholith. The dominant forest type groups are shown in shades of green.....	7
Figure 1.2.	Diagram showing the methodological workflow followed by our study. Includes initial data acquisition sources, data processing steps, and final study results.....	8
Figure 1.3.	Theoretical figure describing the three patterns of expansion using the Landscape Expansion Index (Liu et al., 2010). For each example, the area of the newly detected conifer-present patch is highlighted in black with the associated surrounding 100 m buffer zone. The underlying conifer presence-absence raster represents the cover present at the previous analysis timestep. (A) Infilling shows that > 50% of the newly detected patch buffer zone was forested in the previous timestep. (B) Edge expansion shows that < 50% of the newly detected patch buffer zone was forested in the previous timestep. (C) Leapfrog shows that none of the area within the newly detected patch buffer zone was forested in the previous timestep.....	18
Figure 1.4.	Piecewise generalized linear regression of snow-cover dNDVI through time, comparing Douglas-fir, lodgepole pine, and fir-spruce forest type groups. High-severity patches have been relativized by pre-fire condition and plotted through time relative to fire event year.....	21
Figure 1.5.	Alluvial plot showing fragmentation of total patch area through time within each forest type. Total area of the initial high-severity burn patches, arranged by size class, is plotted on the left of each figure. The total area of reforestation and remaining unforested patches, by size class, are plotted on the right of each figure. Flowlines represent how much area from each initial high-severity burn patch size class has moved into the different divisions after 30-years	23
Figure 1.6.	Boxplot distributions of the proportion of conifer occupancy within patches over 3-year analysis time windows for each forest type group. Trend lines represent locally weighted running line smoother of median occupancy and associated 95% confidence intervals.....	24
Figure 1.7.	Comparison of post-fire conifer expansion patterns between forest type groups (a) Percent of the total area recolonized by conifers detected at each analysis timestep for each forest type group (b) Area Weighted Mean Expansion Index through time for each forest type group. Horizontal line represents the division between growth by expansion (<50) and growth by infill (>50).....	25

CHAPTER 1: CHARACTERIZING 30-YEARS OF CONIFER REGENERATION PATTERNS IN HIGH-SEVERITY WILDFIRES: A SNOW-COVER REMOTE SENSING APPROACH

1.1 Introduction

There has been an increasing number of large wildfires occurring across the Western United States, with rising trends in the size, extent, and duration of fire events since the 1980s (Dennison et al., 2014; Jolly et al., 2015; Picotte et al., 2016). Wildfire intensification has been linked to climatic shifts resulting in warming temperatures, earlier spring snowmelts, and summer moisture deficits (Littell et al., 2009; Westerling et al., 2006). The Northern Rocky Mountains, specifically, have seen the greatest rise in wildfire activity, accounting for 60 percent of the increased frequency of large wildfire events across the West between 1970 and 2003 (Westerling et al., 2006). In this region, wildfire is anticipated to continue increasing in size and frequency, resulting from lengthening fire seasons, shortened fire return intervals, and drier fuel moistures (Morgan et al., 2008; Riley & Loehman, 2016; Westerling et al., 2011). The Northern Rockies have also seen changes to wildfire severity, with trends towards wildfires burning greater areas at high-severity and increasing average severity between 1984 and 2017 (Parks & Abatzoglou, 2020; Picotte et al., 2016). High-severity wildfire is driven primarily by available live fuels in combination with weather, climate, and topography (Birch et al., 2015; Dillon et al., 2011; Keyser & Westerling, 2017; Parks et al., 2018a). It is anticipated that increasing wildfire size and area burned at high-severity may reduce fire heterogeneity to create larger, more simply-shaped, high-severity burn patches (Harvey et al., 2016c).

Wildfire intensification has many wide-ranging impacts on both the environment and society. Wildfire imposes a large economic burden, costing billions of dollars annually from intervention and mitigation efforts, losses to timber and agricultural markets, and impacts on affected local communities (Bayham et al., 2022; Thomas et al., 2017). Furthermore, wildfire imposes social costs from loss of recreation opportunities and cultural connections to natural areas (Englin et al., 1996; Gellman et al., 2022; Vukomanovic & Steelman, 2019). Ecologically, high-severity fire significantly disrupts regional hydrology by increasing runoff, sedimentation, and flooding (Ice et al., 2004; Shakesby & Doerr, 2006). Soil resources are also impacted by fire effects, altering physical, chemical, and biological properties and processes (Certini, 2005; Ice et al., 2004). The loss of forest cover from high-severity burning has implications for many wildlife species, impacting biodiversity and habitat suitability (Fontaine & Kennedy, 2012; Steel et al., 2022). Forest loss from high-severity fire also results in increased carbon emissions and reduces the ability for forest ecosystems to sequester carbon (Loehman, 2020; Sommers et al., 2014).

While fire is an important fixture in the disturbance regimes of the Northern Rocky Mountains, it is unclear how increasing occurrence of high-severity events will impact forest resilience. The forests of the Northern Rockies have historically followed a mixed- to high-severity fire regime, with intensity varying across the elevational gradient that drives species dominance (Gruell, 1985; Schoennagel et al., 2004). The ability for the conifer-dominated forests of the Northern Rocky Mountains to effectively recolonize high-severity patches may be constrained if short-interval reburning precludes sufficient seed source generation (Stevens-Rumann & Morgan, 2016; Turner et al., 2019; Westerling et al., 2011). Increasing prevalence of larger and more simply shaped high-severity patches may also limit recovery by reducing access to seed

sources (Harvey et al., 2016b; Kemp et al., 2016), as conifer seed dispersal is largely limited beyond 100 m from patch edges in Northern Rocky Mountain forests (Kemp et al., 2016). Seedling recruitment may face additional challenges with less-favorable conditions for regeneration success following climate change (Stevens-Rumann et al., 2018). Given the documented limitations on post-fire regeneration, lower elevation trailing-edge ponderosa pine (*Pinus ponderosa*) and Douglas-fir (*Pseudotsuga menziesii*) forests and high-elevation subalpine forests have been identified as showing potentially reduced resilience to wildfire intensification (Davis et al., 2019; Donato et al., 2016; Harvey et al., 2016c; Kemp et al., 2019a; Parks et al., 2019; Turner et al., 2019).

Given the rise of high-severity wildfires and subsequent constraints on conifer regeneration, it is important to characterize how different forests in the Northern Rocky Mountains recolonize high-severity burn patches. Regeneration dynamics post-fire are a fundamental component to inform how disturbance regime changes may impact forest recovery and have significant implications for forest management. Post-fire regeneration is typically described by plot or transect-based field studies assessing seed dispersal distances, seedling densities, and spatial arrangement of regeneration through case studies at relatively small spatial extents (Chambers et al., 2016; Kashian et al., 2004; Kemp et al., 2016; Owen et al., 2017). Field studies have provided valuable information on forest recovery patterns following high-severity burns but can be limited in scope given sampling constraints. The cost of field surveys generally precludes comprehensive assessment of every fire or region, acquiring repeated measurements, or fully characterizing large areas. Given the significance of wildfire intensification, developing

additional data sources should be prioritized to sufficiently evaluate patterns of forest recolonization at the landscape scale.

Remote sensing has proven to be an incredibly important tool in monitoring fire effects and recovery, with the ability to conduct repeated monitoring over extensive areas (Szpakowski & Jensen, 2019). The Landsat program has been a valuable resource for post-fire monitoring with over 50 years of consistent, freely available moderate-resolution satellite imagery. While there have been notable technological advances in relevant satellite spatial (e.g. Sentinel, IKONOS) and spectral resolution (e.g. ASTER, AVIRIS), Landsat remains one of the most widely used tools to monitor post-fire recovery given its accessibility and availability (Chuvieco et al., 2020; Szpakowski & Jensen, 2019). In typical post-fire remote sensing assessments, recovery is measured as a return to pre-fire growing-season vegetation greenness with spectral indices such as the Normalized-Difference Vegetation Index (NDVI) (Szpakowski & Jensen, 2019; White et al., 1996). While growing-season NDVI is a useful measure of vegetation density and greenness, it is not sensitive to what type of vegetation is specifically present. The lack of specificity in growing-season NDVI may overestimate rates of forest recovery by conflating the presence of vegetation with the reestablishment of coniferous tree cover (Bright et al., 2019; Kiel & Turner, 2022; Vanderhoof & Hawbaker, 2018).

Several remote sensing analyses have found success utilizing alternate season imagery to differentiate between forest vegetation types (Dymond et al., 2002; Townsend & Walsh, 2001; Wang et al., 2022; Wolter et al., 1995). Using snow-cover winter imagery has been shown to specifically improve the discrimination of evergreen conifer (hereafter *conifer*) tree presence from other vegetation (Vanderhoof et al., 2021; Wolter et al., 2008). Furthermore, snow-cover

imagery may reduce issues surrounding NDVI saturation at high vegetation densities by reducing overall NDVI spectral reflectance (Sellers, 1985). By using snow as a physical and phenological filter, spectral contributions of vegetation greenness from deciduous or herbaceous vegetation and low-lying evergreen ground cover are diminished. Snow-cover imagery has been successfully utilized to measure post-fire NDVI recovery trends (Vanderhoof et al., 2021; Vanderhoof & Hawbaker, 2018), but has not yet been applied to identify spatial patterns of conifer recolonization. Modeling the presence and absence of conifer regeneration over time using snow-cover imagery can create a more detailed picture of post-fire recovery that includes patterns of growth and proportions of burn patches reforested by conifer species. Pixel-based binary classification can be used to describe post-fire dynamics typically only achieved with field studies, but with the larger temporal and spatial scales of Landsat.

Our research aims to outline the application of snow-cover Landsat imagery to assess conifer regeneration patterns following high-severity wildfire in the Northern Rocky Mountains. We will focus on one of the largest series of high-severity events that occurred in the region following the 1988-1990 North American Drought (Trenberth et al., 1988). Dry conditions led to a series of numerous, high-severity wildfires in 1988 and following years, that include the year of largest mean fire size and 7 of the 38 extreme fire events occurring in the Northern Rocky Mountains and Great Basin between 1984 and 2009 (Lannom et al., 2014). Our study will focus on high-severity fires occurring between 1988 and 1991 to examine post-fire regeneration patterns between several conifer-dominated forest types over a 30-year recovery period in the Northern Rocky Mountains. Our research objectives were to:

1. Evaluate the ability of Landsat and snow-cover remote sensing to detect conifer regeneration following high-severity wildfire.
2. Characterize conifer recolonization patterns and estimate recovery timelines following high-severity wildfire across forest types within the Northern Rocky Mountains.
3. Identify site characteristics of high-severity burn patches that may impact the likelihood of successful conifer recovery 30-years post-fire in the Northern Rocky Mountains.

1.2 Methods

1.2.1 Study Area

The study area was defined as the US Northern Rocky Mountains, comprised of four, conifer-dominated EPA Level-III Ecoregion groups: Canadian Rockies, Northern Rockies, Middle Rockies, and Idaho Batholith (Omernik & Griffith, 2014). The four ecoregions encompass portions of Idaho, Montana, Wyoming, and Washington states (Figure 1.1). At higher elevations, the forests of our study area are comprised of subalpine forests dominated by subalpine fir (*Abies lasiocarpa*) and Engelmann spruce (*Picea engelmannii*) commonly associated with lodgepole pine (*Pinus contorta*) and whitebark pine (*Pinus albicaulis*). Lower to mid-elevation mixed-conifer forests are comprised primarily of Douglas-fir alongside western larch (*Larix occidentalis*), grand fir (*Abies grandis* var. *idahoensis*), ponderosa pine, limber pine (*Pinus flexilis*), lodgepole pine, and quaking aspen (*Populus tremuloides*) (Daubenmire, 1943).

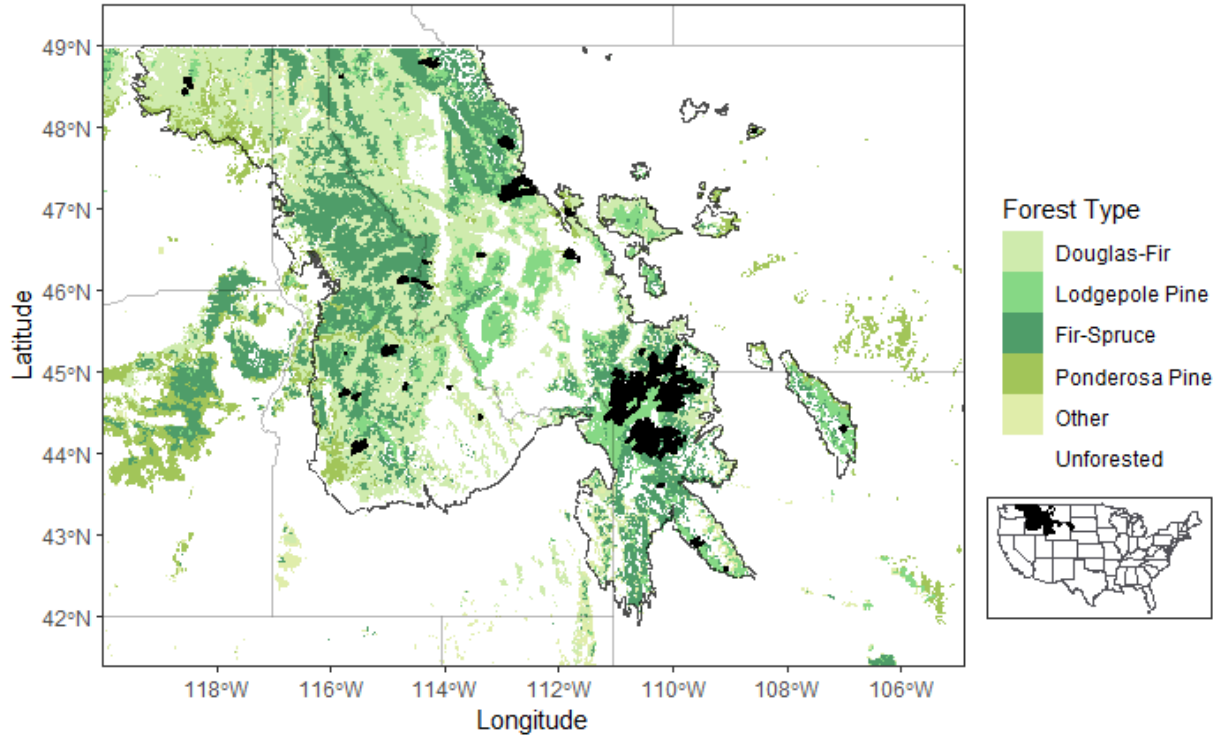


Figure 1.1. Study area map of the 34 high-severity fire events used in our analysis, with fire extents highlighted in black. The dashed boundary line indicates the combined area of the US portion of the EPA Level-III Ecoregion groups Canadian Rockies, Northern Rockies, Middle Rockies, and Idaho Batholith. Dominant forest type groups are shown in shades of green.

Our study specifically focuses on 34 high-severity wildfire complexes totaling 890,000 ha that burned between 1988 and 1991. Mean event elevation ranged between 1000 and 3000 m. Forest types were defined as the dominant conifer vegetation type in each fire perimeter according to the US Forest Service (USFS) National Forest Type Group dataset (Ruefenacht et al., 2008). Eleven events were dominated by fir-spruce-mountain hemlock, nine by lodgepole pine, and fourteen by Douglas-fir. The Landsat imagery for these fire events underwent a series of spectral analysis using pre- and post-burn growing season and snow-covered imagery to characterize high-severity burn patches and their patterns of conifer recolonization (Figure 1.2).

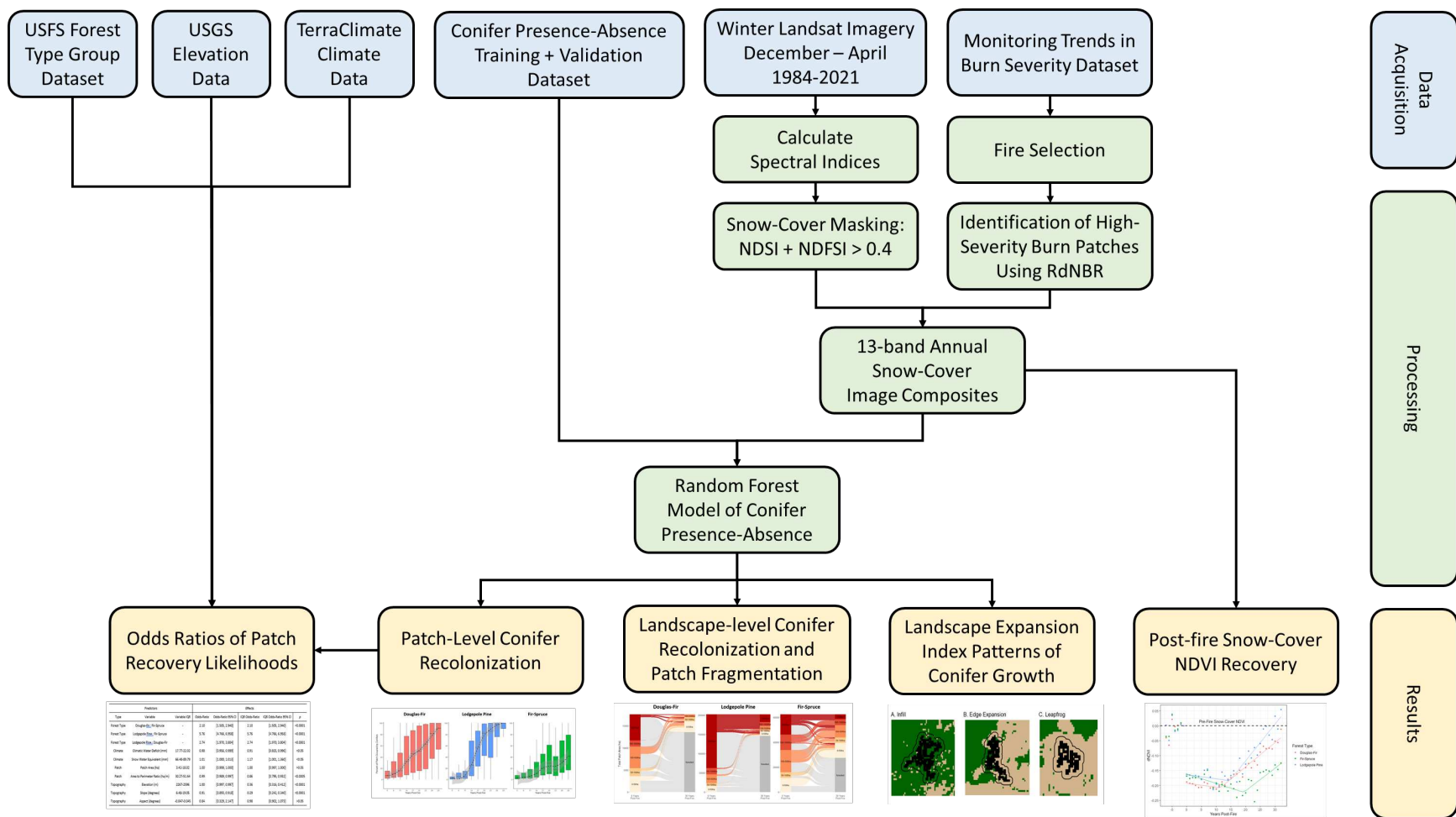


Figure 1.2. Diagram showing the methodological workflow followed by our study. Includes initial data acquisition sources, data processing steps, and final study results.

1.2.2 Fire Selection

Candidate fires were identified from the Monitoring Trends in Burn Severity (MTBS) thematic burn severity and fire perimeter datasets (Eidenshink et al., 2007). Fires were chosen between 1988-1991 to allow for analysis of regeneration over a 30-year post-fire window and to ensure a sufficient record of pre-fire Landsat imagery. To focus on the forested regions of the Northern Rocky Mountains, the dataset was filtered to the bounds of the US portions of the EPA Level-III Ecoregion groups Canadian Rockies, Northern Rockies, Middle Rockies, and Idaho Batholith (Omernik & Griffith, 2014). To increase the likelihood that fires occurred specifically within coniferous forests, further filtering was applied using the US Forest Service's National Forest Type Group dataset (Ruefenacht et al., 2008). Relevant forest type groups included Douglas-fir, ponderosa pine, fir-spruce-mountain hemlock (hereafter *fir-spruce*), and lodgepole pine. Fires were assessed for the relative proportion comprised by each coniferous forest type and removed from analysis if they did not contain at least 25% of a forest type of interest. Final filtering was applied to select fires that had at least 200 ha of high-severity burning as defined by MTBS. Selecting fires with adequate high-severity burning was important to make relevant comparisons between patch sizes and forest types. Ponderosa pine was excluded from further analysis after evaluating fire size requirements, as there were very limited high-severity events within ponderosa pine forests that occurred in our study region and time period.

Fires were then evaluated to ensure they would exhibit patterns of natural regeneration. Areas were removed from analysis if they showed evidence of notable human activity or silvicultural management, such as road systems, buildings, planting rows, or fire lines during visual inspection of high-resolution satellite imagery. Where applicable, fire perimeters were

cross-referenced with the USDA Forest Service Forest Activity Tracking System (FACTS) dataset of reforestation activities to remove areas of known planting or regeneration site preparation on federal lands. Areas of reburning were also excluded from analysis after comparison to the MTBS fire perimeter dataset. Fire selection criteria resulted in a final dataset of 34 large, high-severity wildfire complexes, corresponding to 47 MTBS-defined events, within the Northern Rockies in 1988-1991 (Appendix 1).

1.2.3 Identification of High-Severity Burn Patches

Although MTBS data were used to initially identify high-severity fire events, the reliance on analyst interpretation to determine severity thresholds from dNBR is known to cause fine-scale issues when comparing multiple fires (Kolden et al., 2015; Sparks et al., 2014). Our focus on historic fire events, where precise burn severity field data were often limited for classification, adds additional challenge to achieve accurate dNBR severity thresholds (Miller & Thode, 2007). Consequently, our study identified high-severity burn patches within the selected fires utilizing the Relativized difference Normalized Burn Ratio (RdNBR) (Miller & Thode, 2007). The RdNBR index is based on the Normalized Burn Ratio (NBR), which quantifies burn severity as the difference between the near-infrared (NIR) and short-wave infrared (SWIR) wavelengths (Equation 1; Key & Benson, 2006). SWIR and NIR are particularly sensitive to the presence of vegetation and burned areas, which lend themselves to evaluating post-fire landscapes (White et al., 1996). Burn severity measures are typically calculated by differencing NBR values before and after a fire event, with larger dNBR values corresponding to more severe fire effects (Szpakowski & Jensen, 2019). RdNBR has been shown to have improved success over dNBR at categorizing burn severity across heterogeneous forests, as it normalizes severity by pre-fire

vegetation condition (Equation 2; Cansler & McKenzie, 2012; Miller et al., 2009; Pelletier et al., 2021). Relativized burn severity has been shown to have the greatest improvements relative to dNBR at identifying high-severity burning, as the measure more accurately corresponds to the total loss of vegetation (Miller & Thode, 2007). As our research focuses on high-severity patches in multiple, historic fires across a wide geographic range, RdNBR was identified as the preferred method.

$$NBR = \frac{NIR - SWIR}{NIR + SWIR} \quad (\text{Equation 1})$$

$$RdNBR = \frac{NBR_{prefire} - NBR_{postfire}}{\sqrt{|NBR_{prefire} * 0.001|}} \quad (\text{Equation 2})$$

High-severity patches were delineated by adapting the approach used in Parks et al. 2018b to calculate RdNBR while accounting for phenological differences between image time points. Pre- and post-fire imagery were calculated from the mean annual composite of growing season (day 152-273) Landsat 5 Thematic Mapper (TM) Surface Reflectance imagery for one year preceding and following each fire event. Utilizing annual composites to calculate burn severity has been shown to improve classification accuracy relative to singular pre- and post-fire scenes by standardizing imagery, removing the necessity of analyst image selection, and reducing potential errors from reliance on a singular image (Parks et al., 2018b). To account for any potential phenological differences between the two time points, a dNBR offset adjustment was calculated from the mean dNBR value for all unburned pixels within a 180 m buffer of the fire perimeter. The dNBR offset value was then subtracted from all fire dNBR values to spectrally standardize the two pre- and post-fire image composites (Parks et al., 2018b). High-severity pixels

were identified from RdNBR values greater than 640, a threshold that has been found to align with 95% or greater tree mortality in field-collected data of similar forests (Haffey et al., 2018; Hanson & Odion, 2014; Miller & Thode, 2007).

The patchMorph tool in the patchwoRk package (Girvetz & Greco, 2007) of the R statistical program (R Core Team, 2021) was applied to the RdNBR rasters to delineate individual high-severity patches using 3-cell (90 m) spur and gap thresholds (Collins & Stephens, 2010). Focal filtering has been shown to improve burn severity classification, reduce pixelation, and create more ecologically relevant patches (Miller et al., 2012; Pelletier et al., 2021; Stevens et al., 2018). High-severity patches were removed from our analysis if they were not at least 2.25 ha, or the equivalent of 25 Landsat pixels at 30 m resolution. Finally, patches were assigned to their majority forest type group as defined by the US Forest Service's National Forest Type Group dataset (Ruefenacht et al., 2008). Our patch identification process led to a final dataset of 3,850 high-severity burn patches for analysis.

1.2.4 Snow-cover Landsat Imagery

Snow-cover imagery was assembled from Google Earth Engine (GEE) Landsat 5, 7, and 8 Surface Reflectance data to accommodate the full analysis timeframe. Images taken between December and April were included to ensure sufficient availability of image dates for each winter season, given the challenge of seasonal cloud cover in the region. For each individual image date, several spectral indices associated with vegetation, moisture, snow-cover, and burn severity were calculated: the Normalized Difference Vegetation Index (NDVI; Tucker, 1979), the Enhanced Vegetation Index (EVI; Huete et al., 2002), the Normalized Difference Water Index (NDWI; Gao,

1996), the Normalized Burn Ratio (NBR; García & Caselles, 1991), the Normalized Burn Ratio 2 (NBR2; Key & Benson, 2006), the Normalized Difference Snow Index (NDSI; Hall & Riggs, 2010), and the Normalized Difference Forested Snow Index (NDFSIS; Wang et al., 2015) (Appendix 2).

All selected images were processed to ensure included pixels were representative of true snow-cover conditions. Each image was masked utilizing Landsat's QA pixel bands to exclude pixels containing cloud, cloud shadow, or bodies of water. While the study area is regularly snow-covered within the winter months (December-April), a snow masking process was applied to increase the likelihood that pixels contained snow. Our selected spectral measures of snow-cover, NDSI and NDFSIS, were both employed to identify pixels containing snow-cover as NDSI has greater accuracy in unforested areas and NDFSIS has improved performance within coniferous forests (Wang et al., 2015). Pixels were retained for analysis if they had NDFSIS or NDSI values greater than 0.4, thresholds that are indicative of the presence of snow (Hall et al., 1995; Wang et al., 2015). Finally, annual composite images were created for each fire event and winter season (December-April) by calculating the median pixel values from masked images. Our process of image selection and compositing resulted in an annual series of 13-band images, including six spectral bands and seven derived indices, for each winter season between 1984 and 2022 for each fire event.

1.2.5 Modelling Snow-Cover dNDVI Trajectory

For each winter season evaluated, the mean snow-cover NDVI value was calculated for each high-severity patch. To determine the relative change in NDVI, snow-cover dNDVI was computed by differencing the annual snow-cover NDVI values from the mean pre-fire snow-cover

NDVI. For each forest type group, we used a piecewise generalized linear regression using the segmented package in R (Muggeo, 2008) to explain the variation in dNDVI through time. Piecewise regression was employed to identify when a positive dNDVI slope occurred post-fire, signifying detectable increases in greenness that are assumed to represent coniferous regeneration in the snow-cover imagery. The model was set to identify one breakpoint, using years post-fire as a predictor of dNDVI. Linear trends from the piecewise regressions were used to characterize post-fire dNDVI recovery slopes and estimate recovery timelines within each forest type.

1.2.6 Modelling Conifer Presence and Absence

To characterize spatial patterns of conifer recolonization, a Random Forest classification model was utilized with the snow-cover Landsat composites to classify all pixels within high-severity burn patches as present or absent of conifer tree species through time. Random Forest classifiers are non-parametric and work well with the classification of remotely sensed imagery as they do not rely on normally distributed data and are less susceptible to overfitting (Belgiu & Drăgu, 2016). Model training data were distributed across high-severity patches, with 100 training points allocated to each of the 47 named MTBS fire events ($n = 4,700$). Sample points were stratified across patches with equal weighting between north and south aspects and patch exterior and interior, where interior was defined conservatively as ≥ 150 m from patch edges. Stratification by aspect was implemented to account for potential spectral differences from solar angle. Stratification by patch interior and exterior was utilized to increase the likelihood of the post-fire training data to include more equivalent proportions of regenerating conifer presence and absence. Points were randomly selected within each strata with a minimum of 30 m spacing

to avoid any potential pixel overlap. Training points were then intersected with a 30 m fishnet grid aligned with the Landsat pixels and visually categorized as either present or absent of conifers utilizing a combination of the most recently available National Agricultural Imagery Program (NAIP) and high-resolution imagery available in GEE. Several late-season NAIP data collection years provided at least one snow-cover image for most fire events, which provided useful comparisons of deciduous and coniferous vegetation. A mean composite from three annual snow-cover Landsat composites (2018-2020) was used to train the Random Forest model to accommodate the range of image dates used for training point classification. Using multiple years helps ensure data availability and account for potential variation in annual snow-cover and depth. Furthermore, this range of years is most representative of intact forest structure and capture the widest range of forested conditions on the landscape. Pixel values for all 13 spectral predictors were extracted for each intersecting training data point.

The Random Forest model was developed with the R package `randomForest` (Liaw & Wiener, 2002) to predict conifer presence or absence across all high-severity burn patches. The model used the 13 spectral predictors from the training data points to predict conifer presence-absence. The number of predictors tried at each split (*mtry*) was set at three and the number of trees evaluated (*ntrees*) was 500. Following model creation, independent validation of the 2018-2020 prediction was conducted using 20 points per MTBS event, with 10 points stratified proportionally by predicted area of presence-absence and 5 additional points allocated to each class to ensure a sufficient minimum validation sample size (Olofsson et al., 2014). The performance of the classification was evaluated in a confusion matrix comparing the actual target classes against those predicted by the model. For each misclassified validation point, the percent

of conifer cover was estimated by counting the proportion of conifer containing NAIP pixels within the Landsat fishnet to characterize a threshold of conifer regeneration detectability. Once validated, the model was applied through time to describe the proportion of conifer presence and absence at several timesteps. The snow-cover Landsat imagery was aggregated into 10 timepoints by taking the mean value of the annual composites at three-year intervals. The model was employed to predict conifer presence or absence for each timestep, resulting in 10 conifer presence-absence rasters spanning the 30-year recovery period following each fire event.

1.2.7 Landscape and Patch-level Recolonization

To assess landscape-level patterns of recovery, the initial area of high-severity burn patches was compared to the area of conifer-present (hereafter *forested*) and conifer-absent (hereafter *unforested*) patches 30-years post-fire. Forested and unforested patches were created from contiguous areas of each class from the 30-year timepoint presence-absence prediction raster. Fragmentation was assessed by intersecting forested and unforested patches with the initial high-severity area for each high-severity burn patch. The proportion of conifer presence and absence pixels were assessed for each high-severity patch through time to evaluate the distribution of patch-level recovery for smaller-scale ecological and management implications.

1.2.8 Spatial Patterns of Recolonization

To assess patterns of recolonization, the Landscape Expansion Index (LEI) was employed (Liu et al., 2010). Typically utilized in analyses of urban development, LEI is a metric to characterize spatial patterns of growth. LEI characterizes types and rates of expansion by evaluating the composition of the landscape surrounding areas of new development through

time. As forest recolonization of burn patches relies on similar principles to that of urban development, with dependence on existing structure to expand, LEI lends itself well to evaluate forest recovery. To our knowledge, our research represents the first use of LEI to characterize forest growth outside of an urban setting. Our application of LEI illustrates forest expansion patterns by analyzing the percentage of forested pixels that surround patches of newly detected forest growth (Figure 1.3). Higher values (>50%) of surrounding forest cover indicate patterns of infilling, as the area surrounding the new detection is already predominately forested. Lower values (<50%) indicate patterns of edge expansion, where less than half of the surrounding area is forested (Liu et al., 2010). LEI of 0% represents “leap-frogging”, where none of the area surrounding the new forest detection is forested, indicative of long-distance seed dispersal or growth from serotinous cones. Over time, changes in LEI can be used to document the progression of high-severity patch recolonization as expansion patterns shift from edge expansion to infilling.

To calculate LEI, patches of new conifer detection were identified by differencing the conifer presence-absence rasters at each consecutive timepoint. Each polygon of new conifer detection was buffered at 100 m, our estimated potential seed dispersal distance. Pixel values from the previous timestep were extracted from the buffered ring areas to determine the proportion of area previously forested. The total area and number of instances were evaluated for each expansion type (infill, edge-expansion, leapfrog) to determine the relative contributions of each to post-fire recovery. For each forest type, the Area Weighted Mean Expansion Index (AWMEI) was calculated from all LEI values to describe large-scale patterns of expansion (Liu et al., 2010).

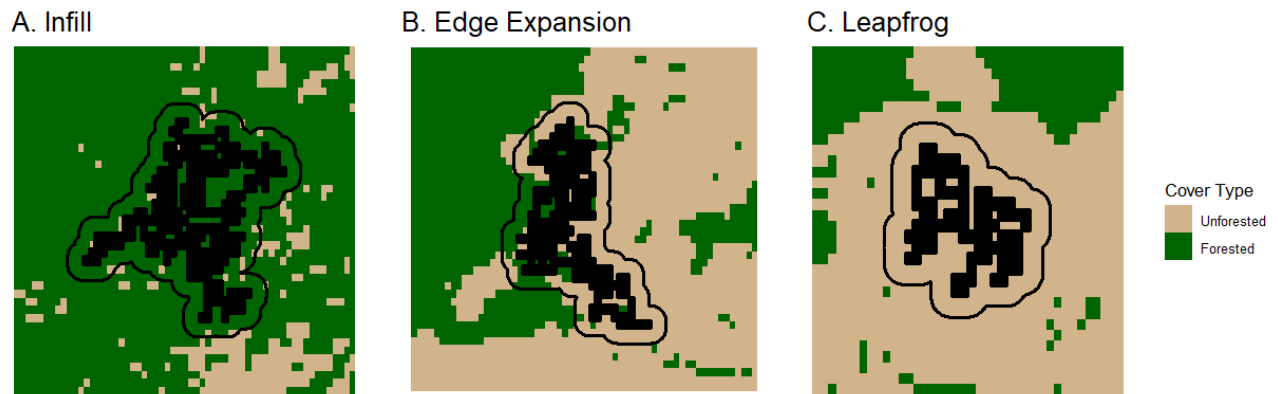


Figure 1.3. Theoretical figure describing the three patterns of expansion using the Landscape Expansion Index (Liu et al., 2010). For each example, the area of the newly detected conifer-present patch is highlighted in black with the associated surrounding 100 m buffer zone. The underlying conifer presence-absence raster represents the cover present at the previous analysis timestep. (A) Infilling shows that > 50% of the newly detected patch buffer zone was forested in the previous timestep. (B) Edge expansion shows that < 50% of the newly detected patch buffer zone was forested in the previous timestep. (C) Leapfrog shows that none of the area within the newly detected patch buffer zone was forested in the previous timestep.

1.2.9 Identifying Characteristics of Recovery

Patch-level characteristics were assessed to evaluate what factors lead to successful recovery 30 years post-fire. Recovery success was defined as a patch reaching 80% recolonization by conifers to correspond with a threshold of near-intact forest structure described in other recovery studies and to balance the distribution of recovery levels across our study area (Viana-Soto et al., 2022; White et al., 2017). A generalized linear logistic regression model was created using the R package rms (Harrell Jr, 2013) to predict 80% patch recovery as a binary value. A suite of predictors variables was selected to characterize biological and environmental controls on forest recovery. Forest type was used as a categorical predictor to account for inherent differences in forest recovery timelines. Patch area and area-to-perimeter ratio were included to describe the importance of patch size and edge-density. Climatic variables Snow Water

Equivalent (SWE) and Climate Water Deficit (DEF) were calculated from the mean patch value from TerraClimate data (Abatzoglou et al., 2018) in a 3-year window (1985-1987) before the fire events occurred. The influence of topographic variables was assessed from the mean patch slope, aspect, and elevation taken from the `elevatr` R package (Hollister et al., 2021). From the full model, odds-ratios were calculated for each predictor to assess the relative change in likelihood for a patch to achieve 80% conifer recovery. The change in odds-ratios across the interquartile range for each predictor was also calculated to provide more relevant comparisons on the relative impact of each predictor across the study area.

1.3 Results

1.3.1. High-severity Burn Patch Distribution

Following the high-severity burn patch identification process, a final dataset of 3,850 high-severity burn patches was created (Table 1.1). Most (51.8%) of the high-severity burn patches were within lodgepole pine, 36.8% within fir-spruce, and 11.3% within Douglas-fir. By area, lodgepole pine represented 71.6%, fir-spruce 22.2% and Douglas-fir 6.3%. Across all forest types, relatively small (<50 ha) patches accounted for the majority (87%) of the total number of patches, however only represented 10.8% of the total area burned at high-severity. Douglas-fir and fir-spruce had more similar distributions of patch number and area between the size classes, while lodgepole pine had a much larger proportion of area (69%) within the largest (>1000 ha) size class.

Table 1.1 Distribution of the number and area of high-severity burn patches evaluated within the study area. Patches are arranged by forest type groups Douglas-fir, fir-spruce, and lodgepole pine and by patch size class.

Forest Type Group	0-50 ha		50-100 ha		100-500 ha		500-1000 ha		1000 ha+	
	Area (ha)	<i>n</i>	Area (ha)	<i>n</i>	Area (ha)	<i>n</i>	Area (ha)	<i>n</i>	Area (ha)	<i>n</i>
Douglas-fir	3,633	387	1,778	25	4,891	21	1,457	2	5,886	3
Fir-spruce	11,308	1,246	4,593	67	17,857	82	12,422	16	16,225	7
Lodgepole pine	15,509	1,725	7,756	112	22,590	109	16,768	24	139,421	23

1.3.2 Snow-Cover dNDVI Recovery and Detection

The piecewise generalized linear regression described overall patterns of snow-cover vegetation greenness following the fire events (Figure 1.4). Douglas-fir and lodgepole pine had adjusted R^2 values of 0.96 and 0.90 respectively, while fir-spruce showed greater variability along the trendline with an R^2 of 0.58. All three forest types saw similar reductions in dNDVI following the fire event in year zero, with model intercepts between -0.162 and -0.193. Initial dNDVI slopes were slightly negative for all forest types before the breakpoint, varying between -0.0032 and -0.0013, although was only significant for fir-spruce. The segmented model breakpoints (hereafter *detection points*) differed with forest type, with a time to detection of 11.5 years for Douglas-fir, 14.6 years for lodgepole pine, and 19.4 years for fir-spruce (Figure 1.4). Post-detection slopes were all positive, with the highest seen in lodgepole pine with 0.0124, followed by 0.0082 in Douglas-fir and 0.0076 in fir-spruce. If future dNDVI trends continue to follow the linear post-detection slope, the estimated recovery time to pre-fire snow-cover NDVI values for the average high-severity patch would be 29.5 years in lodgepole pine, 36.9 years in Douglas-fir, and 48.7 years in fir-spruce.

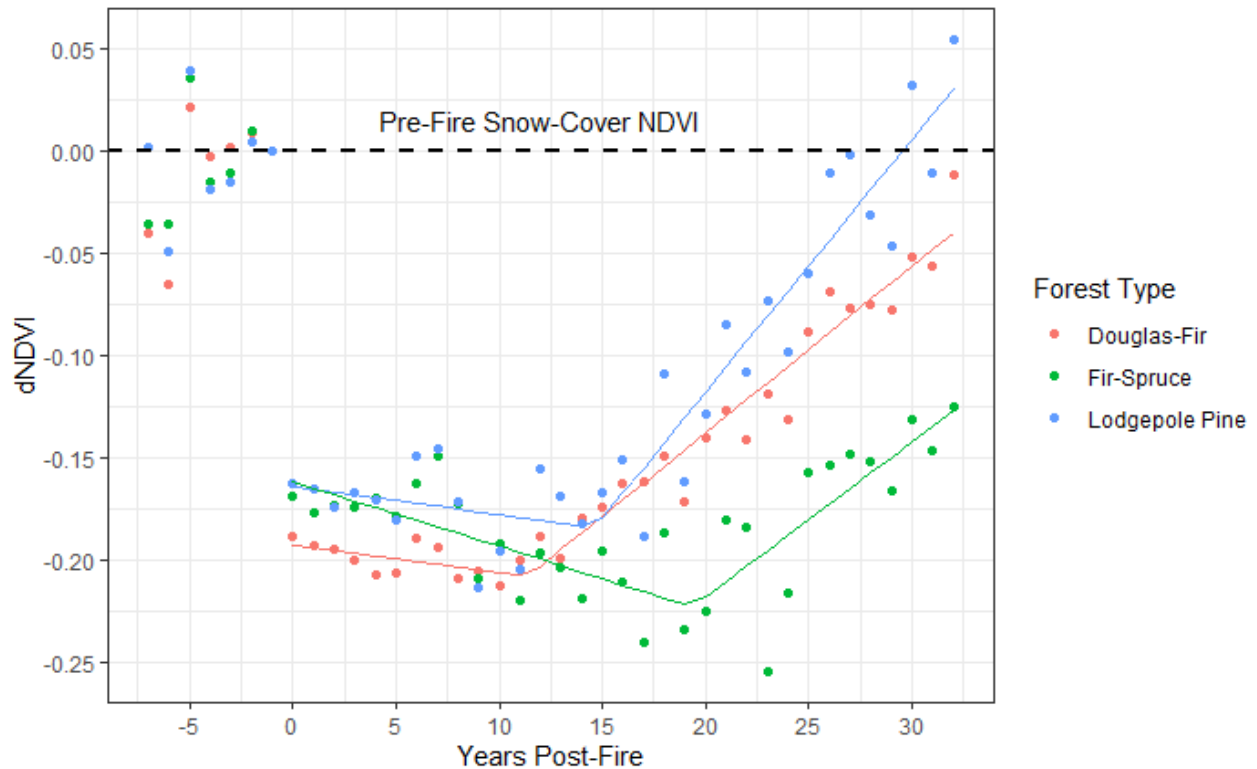


Figure 1.4. Piecewise generalized linear regression of snow-cover dNDVI through time, comparing Douglas-fir, lodgepole pine, and fir-spruce forest type groups. High-severity patches have been relativized by pre-fire condition and plotted through time relative to fire event year.

1.3.3 Conifer Presence-Absence Model Performance

The presence-absence Random Forest model had an initial estimated out-of-bag error rate of 12.0%. The variables of highest importance to the model were the spectral indices NDVI, NDWI, NBR2, and NBR. Accuracy assessment through independent validation showed an overall accuracy rate of 83.2%, with 98.8% accuracy at classifying conifer presence and 58.9% accuracy at classifying conifer absence (Table 1.2). Within the absence misclassifications, where conifer trees were present in the reference class but were incorrectly classified as absent, we found that the majority (72%) of misclassified validation pixels had less than 10% cover of coniferous trees.

A 10% forest cover corresponds to the USFS Forest Inventory and Analysis (FIA) and Food and Agriculture Organization (FAO) of the United Nations definitions of forested, indicating that the preponderance of false negatives occurred where conifer trees were present within an unforested condition. The overall difference in class-level accuracies we documented indicates that our classification of conifer presence may be more conservative than what is present on the landscape.

Table 1.2. Conifer presence-absence Random Forest model error matrix from independent validation expressed in terms of proportion of total area represented by each class. Total (W_i) represents the mapped area proportions and U_i characterizes the user’s accuracy of each class.

Map Classification	Reference Class			
	Conifer Presence	Conifer Absence	Total (W_i)	U_i
Conifer Presence	0.650	0.008	0.658	0.988
Conifer Absence	0.140	0.202	0.342	0.589

1.3.4 Patch Fragmentation and Conifer Recolonization

The landscape-level fragmentation analysis described overall patterns of conifer recovery between forest types for the full study area. Across the 308,000 ha of high-severity burn patches, 65% (202,000 ha) were recolonized by conifers 30 years post-fire (Figure 1.5). The proportion recolonized differed between forest types with 72% of lodgepole pine, 77% of Douglas-fir and 44% of fir-spruce patches reforested. Between patch size classes, patches smaller than 100 ha were 70% reoccupied and patches larger than 100 ha were 65-68% reoccupied. Fragmentation of the high-severity burn patches into smaller unforested patches occurred across all forest types and patch size classes after 30 years (Figure 1.5). Douglas-fir exhibited the greatest fragmentation, with 76% of the unforested area transitioning to smaller patch size classes and

no remaining area in patch sizes larger than 500 ha. Fragmentation within lodgepole pine and fir-spruce patches followed at 61% and 50%, respectively.

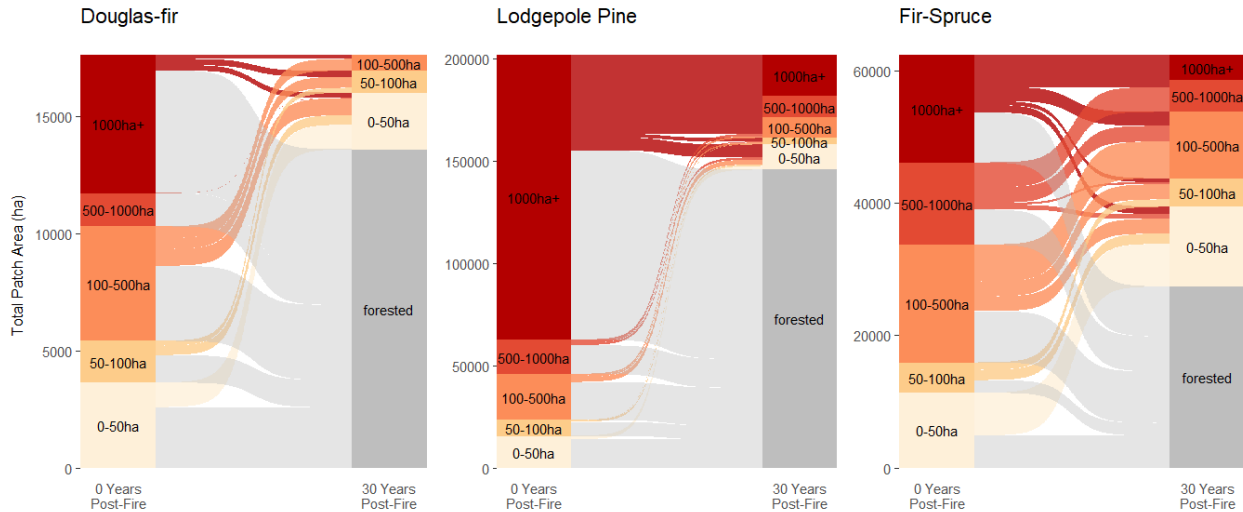


Figure 1.5. Alluvial plot showing fragmentation of the total patch area through time within each forest type. The total area of the initial high-severity burn patches, arranged by size class, is plotted on the left of each figure. The total area of reforestation and remaining unforested patches, by size class, are plotted on the right of each figure. Flowlines represent how much area from each initial high-severity burn patch size class has moved into the different divisions after 30-years.

The patch-level analysis showed the distribution of conifer recolonization across the 3,850 high-severity burn patches (Figure 1.6). Douglas-fir and lodgepole pine patches followed similar recovery trajectories, with median patch occupancy of 91.1% and 100%, respectively, after 30 years (Figure 1.6). The distribution of patch-level occupancy was more compact in lodgepole pine with an interquartile range of 9.8% compared to 46.3% in Douglas-fir. Fir-spruce patches overall had a slower rate of recovery, achieving a median occupancy of 41.3% after 30 years and exhibited the highest degree of variation across patches, with an interquartile range of 62.3%.

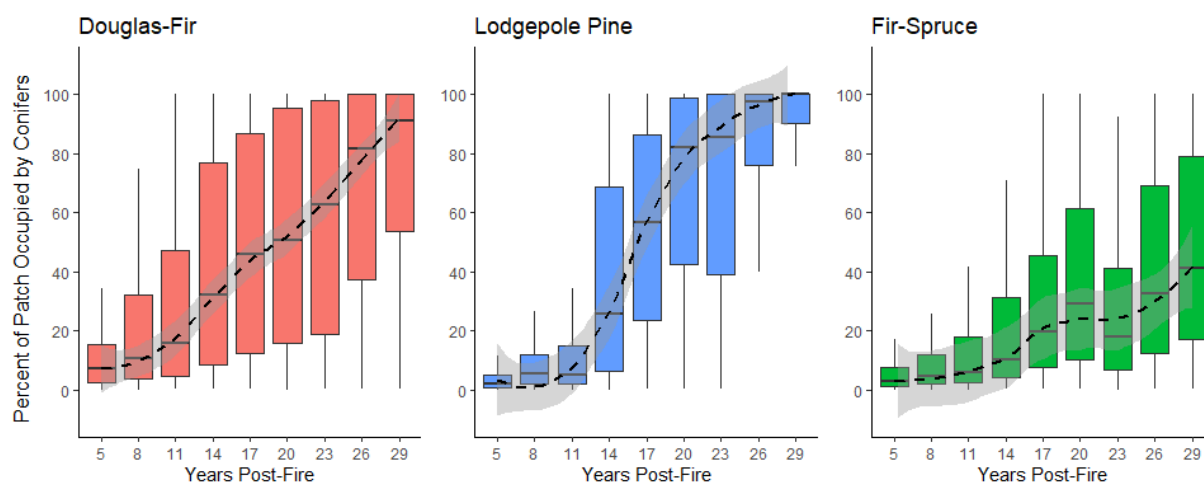


Figure 1.6. Boxplot distributions of the proportion of conifer occupancy within patches over 3-year analysis time windows for each forest type group. Trend lines represent locally weighted running line smoother of median occupancy and associated 95% confidence intervals.

The LEI analysis characterized the expansion patterns between the three forest types. The total reforested area was distributed by the proportion detected at each timepoint post-fire with each forest type. Detection of lodgepole pine occurred in a large pulse, peaking at the 19–21-year timepoint (Figure 1.7a). Douglas-fir had a similar, but slightly more extended pattern, with new detection of forested areas greatest at the 10–15-year timepoints. Fir-spruce patterns differed, with steadily increasing conifer detection over time, with the greatest amount of new detection at the 25–27-year timepoint.

All forest types showed positive trends in AWMEI, matching the predicted recolonization patterns (Figure 1.7b). Overall AWMEI slopes were greatest in lodgepole pine (4.21), indicating a more rapid transition from recovery patterns of edge expansion to infill. Douglas-fir (2.57) and fir-spruce (1.89) slopes were more similar.

Assessment of the recolonized area by expansion type showed no differences between forest types for both edge-expansion and infill. Leapfrogging was a more dominant growth pattern within lodgepole pine than any other forest type across all timepoints. In lodgepole pine, new growth due to leapfrogging appeared in a pulse beginning at, and most notable in the 10–12-year timepoint. At its peak, leapfrogging represented 6% of the total number and 4% of the total area of new conifer detection. Leapfrogging was also present in Douglas-fir and fir-spruce; however, proportions were never larger than 2% of instances at any timepoint and appeared at irregular intervals through time.

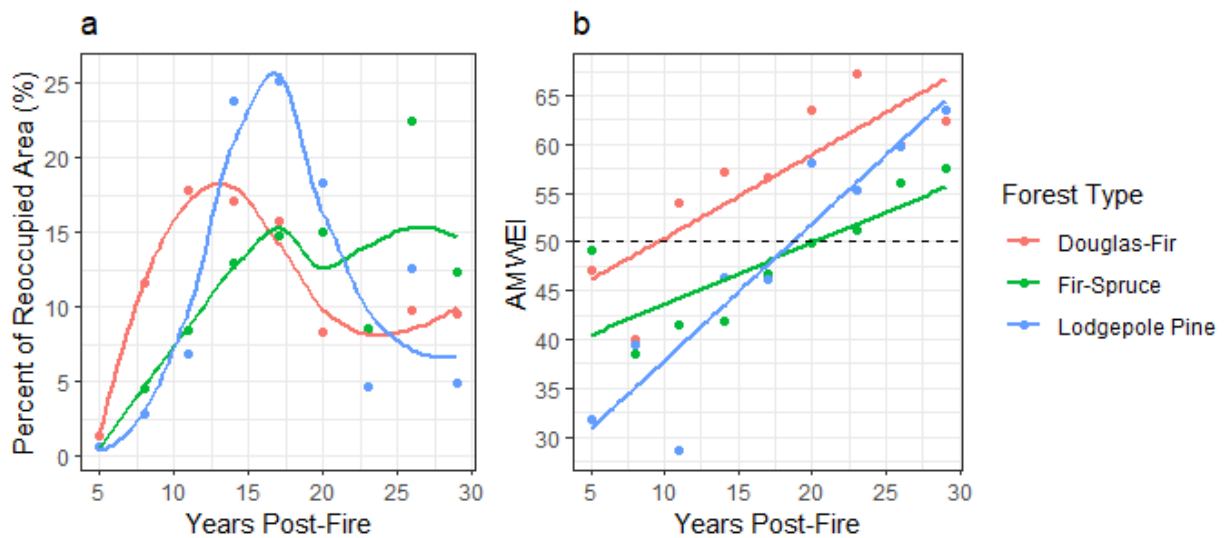


Figure 1.7. Comparison of post-fire conifer expansion patterns between forest type groups (a) Percent of the total area recolonized by conifers detected at each analysis timepoint for each forest type group (b) Area Weighted Mean Expansion Index through time for each forest type group. Horizontal line represents the division between growth by expansion (<50) and growth by infill (>50).

1.3.5 Evaluation of Patch Recovery

The odds-ratios from the generalized linear logistic regression outlined structural, environmental, and biological factors leading to increased likelihood of a patch achieving 80% conifer recovery 30 years post-fire (Table 1.3). Forest type group had a significant effect on determining recovery, with lodgepole pine and Douglas-fir patches respectively associated with a 5.76- and 2.74-times greater likelihood of patch recovery relative to fir-spruce. The two climate variables showed reduced likelihood of recovery within drier sites, with increasing evaporative demand (DEF) and decreasing snowpack (SWE) significantly associated with lower recovery probabilities. In terms of patch structure, increasing patch area-to-perimeter ratio showed significant reductions in probability of recovery, while patch size did not have a significant effect. Increases in the topographic factors of elevation and slope were associated with reduced recovery, while aspect was not identified as a significant predictor.

Comparing the relative change in odds across the interquartile range for each continuous predictor variable can be used to show the relative importance of each within the study area. Topographic variables had the largest odds-ratio magnitude, associated with a 64% and 71% reduction in the likelihood of conifer recovery across the interquartile range of the data. The other significant predictors showed 17% increase in recovery odds across SWE, 9% reduction in recovery odds across DEF, and 14% reduction in recovery odds across area-to-perimeter ratio.

Table 1.3 Odds-ratios from the generalized linear logistic regression model of conifer recovery. Odds-ratios greater than one indicate an increased likelihood of reaching 80% recovery 30 years post-fire, where values less than one indicate a reduced likelihood of recovery. Continuous predictors show the odds-ratio as the change in recovery likelihood for a one unit increase of that predictor. The interquartile range (IQR) odds-ratio shows the change in odds of conifer recovery across the interquartile range of that variable to provide more relevant comparisons between predictors across the study area. Categorical predictors show the relative difference in odds between each pairwise comparison, with the same odds reported for both ratios.

Predictors			Effects				
Type	Variable	Variable IQR	Odds-Ratio	Odds-Ratio 95% CI	IQR Odds-Ratio	IQR Odds-Ratio 95% CI	<i>p</i>
Forest Type	Douglas-Fir : Fir-Spruce	-	2.10	[1.505, 2.940]	2.10	[1.505, 2.940]	<0.0001
Forest Type	Lodgepole Pine : Fir-Spruce	-	5.76	[4.766, 6.958]	5.76	[4.766, 6.958]	<0.0001
Forest Type	Lodgepole Pine : Douglas-Fir	-	2.74	[1.970, 3.804]	2.74	[1.970, 3.804]	<0.0001
Climate	Climatic Water Deficit (mm)	17.77-22.02	0.98	[0.956, 0.999]	0.91	[0.825, 0.996]	<0.05
Climate	Snow Water Equivalent (mm)	66.48-89.79	1.01	[1.000, 1.013]	1.17	[1.001, 1.360]	<0.05
Patch	Patch Area (ha)	3.42-18.02	1.00	[0.999, 1.000]	1.00	[0.997, 1.000]	>0.05
Patch	Area to Perimeter Ratio (ha/m)	30.27-51.64	0.99	[0.989, 0.997]	0.86	[0.795, 0.932]	<0.0005
Topography	Elevation (m)	2267-2596	1.00	[0.997, 0.997]	0.36	[0.316, 0.412]	<0.0001
Topography	Slope (degrees)	6.48-19.05	0.91	[0.893, 0.918]	0.29	[0.242, 0.340]	<0.0001
Topography	Aspect (degrees)	-0.047-0.045	0.84	[0.329, 2.147]	0.98	[0.902, 1.073]	>0.05

1.4 Discussion

1.4.1 Trends of Snow-cover dNDVI Recovery

Snow-cover NDVI was proven to be an effective methodology to assess overall trends in post-fire conifer recovery, similar to previous studies (Vanderhoof et al., 2021). Piecewise regression of post-fire dNDVI allowed us to successfully estimate snow-cover Landsat conifer detection and recovery timelines for each forest type. Estimated dNDVI detection points and recovery slopes generally align with our expectations given the ecologies of the different forest ecosystems.

The 11-19 years immediately following the fire event showed slightly negative snow-cover dNDVI slopes, likely due to continued post-fire mortality and spectral changes from standing dead trees. While most trees are killed directly by wildfire, mortality may continue for several years due to increased abiotic stressors, insect infestations, or excessive fire injuries (Hood & Varner, 2019). Snags may also persist on the landscape for several years post-fire, and slightly alter spectral values as they eventually fall (Russell et al., 2006). Fir-spruce may have seen a longer period of negative slope due to increased post-fire mortality from greater sensitivity to fire-injury (DeNitto et al., 2000) or greater snag longevity found in thinner-barked species such as Engelmann spruce and subalpine fir (Everett et al., 2000). Dominant fir-spruce tree species are estimated to have the majority of snags persist >25 years following wildfire, compared to 15 years in Douglas-fir and lodgepole pine (Everett et al., 2000).

The differences in model breakpoints between forest types are presumed to result largely from the different regeneration mechanisms and timelines for the dominant species. Lodgepole

pine typically demonstrates a singular regeneration pulse in the year following a fire event, as the heating of serotinous cones causes seeds to be released en masse, with decreasing rates of further establishment through 5 years post-fire (Harvey et al., 2016c). Conversely, Douglas-fir, subalpine fir, and Engelmann spruce have more protracted stand initiation, dependent on dispersal by wind and gravity from residual live trees, with seedling establishment peaking at 4-6 years post-fire. Seedling growth rates also differ between species, with the average number of years to reach breast height in the Northern Rockies the fastest at 7 years in lodgepole pine, followed by 11 years in Douglas-fir, 12 years in Engelmann spruce, and up to 18 years for subalpine fir (Ferguson & Carlson, 2010). Growth rates particularly impact detectability when using snow-cover imagery, as greater accumulated snow depth will increase the time required for conifer seedlings to grow above the snow and reach a detectable height. As annual snow depth accumulation increases with elevation (Grundstein & Mote, 2010), we would anticipate a greater lag in detection time in higher elevation forests. Differences in establishment timelines, growth characteristics, and snow-cover predictably resulted in variation in snow-cover dNDVI detection times. The slower establishment time and growth rate of fir-spruce species, typically found at higher-elevations with greater snow-cover, lead to the longest time to detection at 19.4 years. Detection was sooner within lodgepole pine (14.6 years) with faster growth rates and establishment times as well as within Douglas-fir (11.5 years) which is typically found at lower elevations with relatively faster growth rates.

The snow-cover dNDVI recovery trendlines showed overall patterns of conifer resilience following high-severity wildfire, with all forest types progressing towards pre-fire snow-cover NDVI values following detection. The growth rates and establishment characteristics of lodgepole

pine, Douglas-fir, Engelmann spruce, and subalpine fir are important to determine positive post-detection dNDVI recovery slopes. Lodgepole pine exhibits the greatest post-detection slope, aligning with its characteristics of rapid growth and seedling establishment. The dNDVI slopes for Douglas-fir and fir-spruce are more similar, given their relatively protracted seedling establishment and growth. Projecting the post-detection slopes into the future, we were able to estimate the average number of years required to return to pre-fire snow-cover NDVI values. Estimated recovery time varied fairly widely, with the earliest at 29.5 years in lodgepole pine, 36.9 years for Douglas-fir, and 48.7 years for fir-spruce. Our estimates of recovery time are longer than other similar studies evaluating returns to pre-fire spectral indices in the growing season (Bright et al., 2019), likely from the snow-cover imagery excluding deciduous vegetation. Other snow-cover estimates of recovery have found similar discrepancies; assessment over a wider range of burn severities and forest types showed that growing-season estimates of pre-fire NDVI recovery were approximately 5 times faster than that of snow-cover estimates (Vanderhoof et al., 2021).

1.4.2 Evaluating Snow-cover Landsat Detectability

Snow-cover imagery was proven to be a successful technique to classify conifer presence and absence. Despite the moderate 30 m resolution of Landsat, we were able to detect the presence of conifer-specific vegetation at forested levels of cover with >98% accuracy. While our methods were unsuccessful at detecting low (<10%) conifer cover, this implies that our classification of conifer presence is analogous to a more conservative definition of forested rather than the simple presence of individual conifer trees. Other studies have similarly utilized a 10% cover threshold to define forest recovery based on satellite detectability limits and definitions of

forested cover (Bartels et al., 2016; White et al., 2018; Zhao et al., 2016). While variable across study system, analyses of fractional pixel vegetation cover have found similar thresholds of detectability for Landsat (Negrón-Juárez et al., 2011; Sankey & Glenn, 2011; Williams & Raymond, 2002).

The ability to evaluate conifer recovery through a pixel-based approach is a powerful tool to characterize post-disturbance spatial dynamics through time and across broad extents. Employing snow-cover Landsat imagery to classify conifer presence has enabled long-term assessment of post-fire recovery patterns across 34 wildfire events, totaling 308,000 ha of high-severity burn patches. The capacity to quantitatively measure forest recovery across such a wide spatial and temporal extent is incredibly valuable to track post-fire regrowth. While some of the fire events used in our analysis, such as the Yellowstone fires, have received a lot of attention and research, others are not even named events within MTBS. Understanding post-fire stand development is increasingly important given the rise of wildfire activity and intensity, and methods to quantify recovery patterns at a large scale should continue to be developed and adopted.

Spatially representing forest regrowth following fire has the potential to inform other aspects of ecological recovery. Given the large impact high-severity fire has on soil and water resources (Ice et al., 2004; Shakesby & Doerr, 2006), the spatial arrangement of forest growth following fire may be used to help predict hydrological responses following high-severity events. Forest spatial arrangement has further implications for post-fire wildlife habitat suitability and management for species sensitive to high-severity fire. Furthermore, our methods may be

applied to provide better post-fire evaluations of forest growth for carbon sequestration and timber management.

1.4.3 Patterns of Conifer Recolonization

The patterns of high-severity patch fragmentation and recolonization we identified match with the trends seen in snow-cover dNDVI as well as our expectations given the ecologies of our studied forest systems. Recolonization of large, high-severity patches is a process first constrained by seed dispersal distance and second by the time required for recolonizing trees to reach reproductive maturity (Gill et al., 2021; Kemp et al., 2016). Several successive generations of seedling recruitment, growth, and dispersal may be required to recolonize isolated patch interiors. Therefore, recolonization of high-severity burn patches is likely to occur at different intervals based on the biologies of the dominant conifer species. In addition to serotinous cones, lodgepole pine reaches reproductive maturity sooner than the other dominant species, producing viable seed after 5-15 years, as opposed to 12-15 years in Douglas-fir, 15-40 years in Engelmann spruce and 20 years subalpine fir (Hood et al., 2018). While seed dispersal has been found to be exceedingly constrained beyond 100 m from patch edges in similar forest systems (Gill et al., 2021; Kemp et al., 2016), the ability for individual species to disperse by wind and gravity is much further for Douglas-fir, subalpine fir, and Engelmann spruce than lodgepole pine (Hood et al., 2018). Dispersal constraints, alongside aforementioned species growth rates and seedling establishment times, constrain high-severity patch recolonization.

The results of the patch fragmentation analysis show that the majority of the total area burned at high-severity (65%) has returned to a forested condition 30-years post-fire.

Recolonization was much greater within Douglas-fir (77%) and lodgepole pine (72%) forests relative to fir-spruce (44%). Across patch size classes, we saw significant proportions (67%) of large (>500ha) high-severity burn patches, that are of the greatest concern for management, fragment into smaller unforested patches or were successfully reforested. The remainder of these large, unforested patches primarily persist in fir-spruce and lodgepole pine. The lodgepole pine persistence is likely due to the sheer size of burn patches that occurred within the Yellowstone fires, some as large as 23,000 ha. Large patches within lodgepole pine have fragmented and reforested rapidly when considering their size, but some large fragments still exist. The larger patches within fir-spruce are more likely a result of the slower growth rate, establishment time, and time to maturity of subalpine fir and Engelmann spruce limiting recolonization. While slower recovery of fir-spruce is expected given regeneration constraints, it does signify potentially reduced resilience to increasing high-severity wildfire events.

Comparing the patch-level recolonization analysis to the landscape-level trends shows that the majority of the remaining unforested area persists in fewer, large patches for Douglas-fir and lodgepole pine. This pattern is the most extreme in lodgepole pine, where the median patch is 100% forested yet 28% of the total area remains unforested. As fir-spruce showed more equivalent levels of recovery across all patch size classes, the patch-level distributions did not vary greatly from the landscape-level recovery. The wide occupancy distribution of fir-spruce and Douglas-fir patches shows that an extensive range of recovery conditions are prevalent across the landscape. The range of patch-level recolonization we documented indicates that lodgepole pine is more successfully recovering following high-severity fire across the full range of study

conditions in the Northern Rockies, where fir-spruce and Douglas-fir may be more locally constrained by environmental conditions.

The patterns of landscape and patch-level recovery we documented are explained and supported by the LEI and AWMEI trends across forest types. The AWMEI slopes are the greatest in lodgepole pine, indicating that these forests most effectively transition from patterns of edge expansion to infill. With faster establishment, growth, and dispersal rates, lodgepole pine is well-equipped to quickly recolonize high-severity burn patches. These characteristics are likely greatly enhanced by serotinous cones that provide rapid seedling regeneration and increase amount of growth due to leapfrogging. The regeneration pulse from serotinous cones is identifiable in the LEI analysis, with a large amount of new growth from leapfrogging detected around 10 years post-fire. While leapfrogging represents a relatively small proportion of total recolonization, it is capable of a disproportionate effect on recolonization speed. Leapfrog patches of forest growth may act as seed source islands and enable recolonization of patch interiors much sooner than if they were limited to dispersal from parent trees on patch edges. This also aligns with the high rate of fragmentation seen in lodgepole pine, as expansion is occurring from seed sources within patch interiors as well as patch edges. In contrast, the AMWEI slopes also reflect the slower rate of encroachment within fir-spruce. Slower establishment, growth, and dispersal constrain the ability of Engelmann spruce and subalpine fir to encroach into patch interiors, evidenced by the relatively shallow AMWEI slope. Expansion limitations within fir-spruce forests are likely responsible for the larger proportions of unforested area and reduced fragmentation we documented within fir-spruce forests.

1.4.4 Characteristics of Recovered Patches and Implications for Resilience

While our analyses documented overall patterns of conifer resilience, we identified areas within the Northern Rockies that had reduced likelihoods of conifer recovery after 30 years. Predictably, our odds-ratio analysis identified fir-spruce as having reduced likelihood of recovery relative to Douglas-fir and lodgepole pine. Slower growth, seed production, and establishment constrained fir-spruce recolonization and limited recovery at 30-years post-fire. Our characterization of slower post-fire recolonization within fir-spruce forests generally aligns with other field-based post-fire assessments (Harvey et al., 2016a; Stevens-Rumann et al., 2018). Slower post-fire recovery of fir-spruce forests has historically maintained resilience with a fire regime of infrequent (>200yr), high-severity events (Schoennagel et al., 2004). Increasing wildfire extent and shortening return intervals within subalpine forests may, however, pose challenges for future forest recovery (Gill et al., 2021; Harvey et al., 2016b; Stevens-Rumann & Morgan, 2016).

Our recovery odds analysis also identified that high-severity patches located in drier climates, with lower snowpack and higher evaporative demand, had reduced recovery likelihoods of conifer recovery. This finding aligns with other studies across the Western United States that have shown limited seedling regeneration in hotter and drier conditions (Harvey et al., 2016a; Kemp et al., 2019b; Stevens-Rumann et al., 2018). Again, while our research has documented patterns of conifer resilience in the Northern Rockies, these results suggest increasingly unsuccessful long-term conifer recovery as climate conditions become more adverse to seedling success.

We found that patch configuration, rather than patch size, was significant in determining post-fire recovery likelihood. Larger, contiguous areas burned at high-severity with a more heterogeneous, high-edge density configuration would predictably provide greater access to seed sources than a comparably smaller, homogenous, low-edge density burn patch. The importance of high-edge density we documented aligns with prior field-based research showing that heterogeneity has been important in maintaining post-fire resilience in the Northern Rocky Mountains (Clark-Wolf et al., 2022; Kemp et al., 2016; Kiel & Turner, 2022). Fires specifically used in our analysis exhibited notable heterogeneity, which has been suggested to have supported their successful post-fire recovery (Schoennagel et al., 2008; Turner et al., 1999). With predicted declines in the heterogeneity of burn severity in the Northern Rockies (Harvey et al., 2016b) our findings would also suggest that conifer resilience to high-severity wildfire may be reduced in the future. We suggest that, where appropriate, management efforts be directed towards high-severity burn patches meeting characteristics we found to be associated with reduced conifer recovery.

1.4.5 Limitations and Future Directions

While snow-cover Landsat was proven to be successful for our applications, we identified several limitations and opportunities for future use. As regular winter snow-cover is required to successfully employ these methods, areas with sparse or irregular snow may encounter challenges acquiring sufficient images for analysis. Additionally, snow-cover Landsat imagery would be best utilized in longer-term assessments of post-fire recovery, given the identified lag in conifer detection time. As we were not successful at identifying conifer presence at less than

10% conifer cover and would anticipate difficulties with detectability when applying our classification methods to low-density conifer systems. Higher spatial resolution satellites could conceivably be employed to increase forest detection within areas of low tree cover. If a smaller suite of fires or analysis timepoints were being considered, analysts could additionally select image dates to correspond to lower snow-depths or time since snow event to further improve detection. The conifer detectability thresholds and detectability lags due to snow-cover we identified should be considered when interpreting the results of our analyses.

While our study was successful at characterizing conifer recolonization, snow-cover remote sensing methods alone are not able to characterize all aspects of post-fire forest recovery. Unaided, snow-cover imagery cannot evaluate the recovery of deciduous conifer (i.e. *Larix* spp) or broadleaf tree species. Employing growing-season imagery alongside snow-cover imagery may offer opportunities to evaluate both evergreen conifer and deciduous forest components (Vanderhoof et al., 2021). As our methods were focused on identifying a return of conifer presence, they were not able to characterize post-fire forest structure or composition. Studies have had success using Landsat in combination with LiDAR to measure both forest spectral and structural recovery (Bolton et al., 2015; McCarley et al., 2017; Szpakowski & Jensen, 2019; Viana-Soto et al., 2022; Wulder et al., 2009). Others have paired moderate resolution imagery with field collected data, such as the FIA, to identify forest composition across broad spatial scales (Obata et al., 2021; Ruefenacht et al., 2008; Song et al., 2007; Thapa et al., 2020; Tinkham et al., 2018). Similar approaches could be utilized in concert with snow-cover Landsat imagery to evaluate post-fire forest composition and structure.

Further research into conifer recovery patterns should be pursued across a wider range of time periods and regions of the Western United States. The methods we utilized should be adapted to other conifer-dominated forest ecosystems to similarly compare recovery trends following disturbance events. Analyses should be prioritized in areas with limited long-term field studies or at increased risk of regeneration failure. Comparing recovery trends to more recent fire events would help identify changes to resilience under changing climate and understand implications for increased high-severity wildfire events.

1.5 Conclusion

Our study found that snow-cover Landsat imagery can be successfully utilized to evaluate conifer-specific regeneration following high-severity fire. Consistent with previous research, we found that snow-cover NDVI is an effective method to track post-fire conifer regeneration at a landscape scale, produce ecologically consistent results, and avoid confusion with herbaceous vegetation that can occur when using growing-season imagery. Our study is the first to utilize remotely-sensed snow-cover imagery to spatially model the presence of conifer regeneration and outline the detectability limits of these techniques. Greater than 98% detection accuracy was achieved for identifying conifer regeneration presence in a Landsat pixel, with the preponderance of misclassified conifer-absent pixels having <10% regeneration cover. Such high model reliability suggests that snow-cover remote sensing can be used to provide a clearer picture of post-fire regeneration dynamics and better evaluate post-fire forest recovery.

Conifer regeneration modelling with snow-cover imagery provided opportunities to describe conifer recolonization and fragmentation of high-severity burn patches at the landscape

and patch-level. We were able to quantify spatial patterns of expansion with the first known utilization of the Landscape Expansion Index to characterize how conifers reoccupy high-severity burn patches. Our research has constructed a more detailed picture of long-term post-fire forest recovery for lodgepole pine, Douglas-fir, and fir-spruce forests in the Northern Rocky Mountains, demonstrating differences in the rate and mechanism of conifer recolonization.

Finally, we were able to use our conifer regeneration models to identify high-severity burn patches with reduced likelihoods of conifer recovery in the Northern Rocky Mountains. Analysis identified climate, topography, patch characteristics, and forest types associated with reduced recovery. Given ecological implications of wildfire intensification, identifying site conditions that are at risk of reduced conifer resilience is imperative.

Cited Works

Abatzoglou, J. T., Dobrowski, S. Z., Parks, S. A., & Hegewisch, K. C. (2018). TerraClimate, a high-resolution global dataset of monthly climate and climatic water balance from 1958-2015. *Scientific Data*, 5. <https://doi.org/10.1038/sdata.2017.191>

Bartels, S. F., Chen, H. Y. H., Wulder, M. A., & White, J. C. (2016). Trends in post-disturbance recovery rates of Canada's forests following wildfire and harvest. In *Forest Ecology and Management*, 361, 194–207. <https://doi.org/10.1016/j.foreco.2015.11.015>

Bayham, J., Yoder, J. K., Champ, P. A., & Calkin, D. E. (2022). The economics of wildfire in the United States. *Annu. Rev. Resour. Econ.*, 14, 379–401. <https://doi.org/10.1146/annurev-resource-111920>

Belgiu, M., & Drăgu, L. (2016). Random forest in remote sensing: A review of applications and future directions. In *ISPRS Journal of Photogrammetry and Remote Sensing*, 114, 24–31. <https://doi.org/10.1016/j.isprsjprs.2016.01.011>

Birch, D. S., Morgan, P., Kolden, C. A., Abatzoglou, J. T., Dillon, G. K., Hudak, A. T., & Smith, A. M. S. (2015). Vegetation, topography and daily weather influenced burn severity in central Idaho and western Montana forests. *Ecosphere*, 6(1). <https://doi.org/10.1890/ES14-00213.1>

Bolton, D. K., Coops, N. C., & Wulder, M. A. (2015). Characterizing residual structure and forest recovery following high-severity fire in the western boreal of Canada using Landsat time-

series and airborne lidar data. *Remote Sensing of Environment*, 163, 48–60.

<https://doi.org/10.1016/j.rse.2015.03.004>

Bright, B. C., Hudak, A. T., Kennedy, R. E., Braaten, J. D., & Henareh Khalyani, A. (2019).

Examining post-fire vegetation recovery with Landsat time series analysis in three western North American forest types. *Fire Ecology*, 15(1). <https://doi.org/10.1186/s42408-018-0021-9>

Cansler, C. A., & McKenzie, D. (2012). How robust are burn severity indices when applied in a new region? Evaluation of alternate field-based and remote-sensing methods. *Remote Sensing*, 4(2), 456–483. <https://doi.org/10.3390/rs4020456>

Certini, G. (2005). Effects of fire on properties of forest soils: A review. *Oecologia*, 143(1), 1–10. <https://doi.org/10.1007/s00442-004-1788-8>

Chambers, M. E., Fornwalt, P. J., Malone, S. L., & Battaglia, M. A. (2016). Patterns of conifer regeneration following high severity wildfire in ponderosa pine – dominated forests of the Colorado Front Range. *Forest Ecology and Management*, 378, 57–67. <https://doi.org/10.1016/j.foreco.2016.07.001>

Chuvieco, E., Aguado, I., Salas, J., García, M., Yebra, M., & Oliva, P. (2020). Satellite remote sensing contributions to wildland fire science and management. *Current Forestry Reports*, 6(2), 81–96. <https://doi.org/10.1007/s40725-020-00116-5>

- Clark-Wolf, K., Higuera, P. E., & Davis, K. T. (2022). Conifer seedling demography reveals mechanisms of initial forest resilience to wildfires in the northern Rocky Mountains. *Forest Ecology and Management*, 523. <https://doi.org/10.1016/j.foreco.2022.120487>
- Collins, B. M., & Stephens, S. L. (2010). Stand-replacing patches within a “mixed severity” fire regime: Quantitative characterization using recent fires in a long-established natural fire area. *Landscape Ecology*, 25(6), 927–939. <https://doi.org/10.1007/s10980-010-9470-5>
- Daubenmire, R. F. (1943). Vegetational zonation in the Rocky Mountains. *The Botanical Review*, 9(6), 325–393. <https://doi.org/https://doi.org/10.1007/BF02872481>
- Davis, K. T., Dobrowski, S. Z., Higuera, P. E., Holden, Z. A., Veblen, T. T., Rother, M. T., Parks, S. A., Sala, A., & Maneta, M. P. (2019). Wildfires and climate change push low-elevation forests across a critical climate threshold for tree regeneration. *PNAS*, 116(13), 6193–6198. <https://doi.org/10.5061/dryad.pc3f9d8>
- DeNitto, G., Cramer, B., Gibson, K., Lockman, B., McConnell, T., & Stipe, L. (2000). Survivability and deterioration of fire-injured trees in the northern rocky mountains : a review of the literature. *The Bark Beetles, Fuels, and Fire Bibliography*, 1.
- Dennison, P. E., Brewer, S. C., Arnold, J. D., & Moritz, M. A. (2014). Large wildfire trends in the western United States, 1984-2011. *Geophysical Research Letters*, 41(8), 2928–2933. <https://doi.org/10.1002/2014GL059576>

- Dillon, G. K., Holden, Z. A., Morgan, P., Crimmins, M. A., Heyerdahl, E. K., & Luce, C. H. (2011). Both topography and climate affected forest and woodland burn severity in two regions of the western US, 1984 to 2006. *Ecosphere*, 2(12). <https://doi.org/10.1890/ES11-00271.1>
- Donato, D. C., Harvey, B. J., & Turner, M. G. (2016). Regeneration of montane forests 24 years after the 1988 Yellowstone fires: A fire-catalyzed shift in lower treelines? *Ecosphere*, 7(8). <https://doi.org/10.1002/ecs2.1410>
- Dymond, C. C., Mladenoff, D. J., & Radeloff, V. C. (2002). Phenological differences in Tasseled Cap indices improve deciduous forest classification. *Remote Sensing of Environment*, 80(3), 460–472. [https://doi.org/10.1016/S0034-4257\(01\)00324-8](https://doi.org/10.1016/S0034-4257(01)00324-8)
- Eidenshink, J., Schwind, B., Brewer, K., Zhu, Z.-L., Quayle, B., & Howard, S. (2007). A project for monitoring trends in burn severity. *Fire Ecology*, 3(1), 3-21. <https://doi.org/10.4996/fireecology.0301003>
- Englin, J., Boxall, P. C., Chakraborty, K., & Watson, D. O. (1996). Valuing the impacts of forest fires on backcountry forest recreation. *Forest Science*, 42(4), 450–455. <https://doi.org/10.1093/forestscience/42.4.450>
- Everett, R., Lehmkuhl, J., Schellhaas, R., Ohlson, P., Keenum, D., Riesterer, H., & Spurbeck, D. (2000). Snag dynamics in a chronosequence of 26 wildfires on the East Slope of the Cascade Range in Washington State, USA. *International Journal of Wildland Fire*, 9(4), 223–234. <https://doi.org/10.1071/wf00011>

Ferguson, D. E., & Carlson, C. E. (2010). *Height-age relationships for regeneration-size trees in the Northern Rocky Mountains, USA*. US Department of Agriculture, Forest Service, Rocky Mountain Research Station.

Fontaine, J. B., & Kennedy, P. L. (2012). Meta-analysis of avian and small-mammal response to fire severity and fire surrogate treatments in U.S. Fire-prone forests. *Ecological Applications*, 22(5), 1547–1561. <https://doi.org/10.1890/12-0009.1>

Gao, B.-C. (1996). NDWI a normalized difference water index for remote sensing of vegetation liquid water from space. *Remote Sens. Environ*, 7212, 257–266.
[https://doi.org/10.1016/S0034-4257\(96\)00067-3](https://doi.org/10.1016/S0034-4257(96)00067-3)

García, M. J. L., & Caselles, V. (1991). Mapping burns and natural reforestation using thematic mapper data. *Geocarto International*, 6(1), 31–37.
<https://doi.org/10.1080/10106049109354290>

Gellman, J., Walls, M., & Wibbenmeyer, M. (2022). Wildfire, smoke, and outdoor recreation in the western United States. *Forest Policy and Economics*, 134.
<https://doi.org/10.1016/j.forpol.2021.102619>

Gill, N. S., Hoecker, T. J., & Turner, M. G. (2021). The propagule doesn't fall far from the tree, especially after short-interval, high-severity fire. *Ecology*, 102(1).
<https://doi.org/10.1002/ecy.3194>

- Girvetz, E. H., & Greco, S. E. (2007). How to define a patch: A spatial model for hierarchically delineating organism-specific habitat patches. *Landscape Ecology*, 22(8), 1131–1142. <https://doi.org/10.1007/s10980-007-9104-8>
- Gruell, G. E. (1985). Fire on the early western landscape: an annotated record of wildland fires 1776-1900. *Northwest Science*, 59(2), 97–107.
- Grundstein, A., & Mote, T. (2010). Trends in average snow depth across the Western United States. *Physical Geography*, 31(2), 172–185. <https://doi.org/10.2747/0272-3646.31.2.172>
- Haffey, C., Sisk, T. D., Allen, C. D., Thode, A. E., & Margolis, E. Q. (2018). Limits to ponderosa pine regeneration following large high-severity forest fires in the United States Southwest. *Fire Ecology*, 14(1), 143–163. <https://doi.org/10.4996/fireecology.140114316>
- Hall, D. K., & Riggs, G. A. (2010). Normalized-difference snow index (NDSI). *Encyclopedia of Snow, Ice and Glaciers*. https://doi.org/https://doi.org/10.1007/978-90-481-2642-2_376
- Hall, D. K., Riggs, G. A., & Salomonson, V. V. (1995). Development of methods for mapping global snow cover using moderate resolution imaging spectroradiometer data. *Remote Sensing of Environment*, 54(2), 127–140.
- Hanson, C. T., & Odion, D. C. (2014). Is fire severity increasing in the Sierra Nevada, California, USA? *International Journal of Wildland Fire*, 23(1), 1–8. <https://doi.org/10.1071/WF13016>
- Harrell Jr, F. (2013). rms: Regression modeling strategies. *R Package Version*, 5(2).

- Harvey, B. J., Donato, D. C., & Turner, M. G. (2016a). Burn me twice, shame on who? Interactions between successive forest fires across a temperate mountain region. *Ecology*, 97(9), 2272–2282. <https://doi.org/10.1002/ecy.1439>
- Harvey, B. J., Donato, D. C., & Turner, M. G. (2016b). Drivers and trends in landscape patterns of stand-replacing fire in forests of the US Northern Rocky Mountains (1984–2010). *Landscape Ecology*, 31(10), 2367–2383. <https://doi.org/10.1007/s10980-016-0408-4>
- Harvey, B. J., Donato, D. C., & Turner, M. G. (2016c). High and dry: Post-fire tree seedling establishment in subalpine forests decreases with post-fire drought and large stand-replacing burn patches. *Global Ecology and Biogeography*, 25(6), 655–669. <https://doi.org/10.1111/geb.12443>
- Hollister, J., Shah, T., Robitaille, A., Beck, M., & Johnson, M. (2021). *elevatr: Access Elevation Data from Various APIs*. <https://doi.org/10.5281/zenodo.5809645>
- Hood, S. M., Abrahamson, I., & Cansler, C. A. (2018). *Fire Resistance and Regeneration Characteristics of Northern Rockies Tree Species*. Fire Effects Information System,[Online]. USDA Forest Service, Rocky Mountain Research Station, Missoula Fire Sciences Laboratory (Producer). <https://www.fs.fed.us/database/feis/pdfs/other/FireResistRegen.html>.
- Hood, S. M., & Varner, J. M. (2019). Post-fire Tree Mortality. In *Encyclopedia of Wildfires and Wildland-Urban Interface (WUI) Fires* (pp. 1–10). Springer International Publishing. https://doi.org/10.1007/978-3-319-51727-8_252-1

- Huete, A., Didan, K., Miura, T., Rodriguez, E. P., Gao, X., & Ferreira, L. G. (2002). Overview of the radiometric and biophysical performance of the MODIS vegetation indices. *Remote Sensing of Environment*, *83*, 195–213. [https://doi.org/10.1016/S0034-4257\(02\)00096-2](https://doi.org/10.1016/S0034-4257(02)00096-2)
- Ice, G. G., Neary, D. G., & Adams, P. W. (2004). Effects of wildfire on soils and watershed processes. *Journal of Forestry*, *102*(6), 16–20.
- Jolly, W. M., Cochrane, M. A., Freeborn, P. H., Holden, Z. A., Brown, T. J., Williamson, G. J., & Bowman, D. M. J. S. (2015). Climate-induced variations in global wildfire danger from 1979 to 2013. *Nature Communications*, *6*. <https://doi.org/10.1038/ncomms8537>
- Kashian, D. M., Tinker, D. B., Turner, M. G., & Scarpace, F. L. (2004). Spatial heterogeneity of lodgepole pine sapling densities following the 1988 fires in Yellowstone National Park, Wyoming, USA. *Canadian Journal of Forest Research*, *34*(11), 2263–2276. <https://doi.org/10.1139/X04-107>
- Kemp, K. B., Higuera, P. E., & Morgan, P. (2016). Fire legacies impact conifer regeneration across environmental gradients in the U.S. northern Rockies. *Landscape Ecology*, *31*(3), 619–636. <https://doi.org/10.1007/s10980-015-0268-3>
- Kemp, K. B., Higuera, P. E., Morgan, P., & Abatzoglou, J. T. (2019a). Climate will increasingly determine post-fire tree regeneration success in low-elevation forests, Northern Rockies, USA. *Ecosphere*, *10*(1). <https://doi.org/10.1002/ecs2.2568>

- Kemp, K. B., Higuera, P. E., Morgan, P., & Abatzoglou, J. T. (2019b). Climate will increasingly determine post-fire tree regeneration success in low-elevation forests, Northern Rockies, USA. *Ecosphere*, *10*(1). <https://doi.org/10.1002/ecs2.2568>
- Key, C. H., & Benson, N. C. (2006). Landscape assessment (LA). *FIREMON: Fire effects monitoring and inventory system*, *164*, LA-1.
- Keyser, A., & Westerling, A. L. (2017). Climate drives inter-annual variability in probability of high severity fire occurrence in the western United States. *Environmental Research Letters*, *12*(6). <https://doi.org/10.1088/1748-9326/aa6b10>
- Kiel, N. G., & Turner, M. G. (2022). Where are the trees? Extent, configuration, and drivers of poor forest recovery 30 years after the 1988 Yellowstone fires. *Forest Ecology and Management*, *524*. <https://doi.org/10.1016/j.foreco.2022.120536>
- Kolden, C. A., Smith, A. M. S., & Abatzoglou, J. T. (2015). Limitations and utilisation of Monitoring Trends in Burn Severity products for assessing wildfire severity in the USA. *International Journal of Wildland Fire*, *24*(7), 1023–1028. <https://doi.org/10.1071/WF15082>
- Lannom, K. O., Tinkham, W. T., Smith, A. M. S., Abatzoglou, J., Newingham, B. A., Hall, T. E., Morgan, P., Strand, E. K., Paveglio, T. B., Anderson, J. W., & Sparks, A. M. (2014). Defining extreme wildland fires using geospatial and ancillary metrics. *International Journal of Wildland Fire*, *23*(3), 322–337. <https://doi.org/10.1071/WF13065>

Liaw, A., & Wiener, M. (2002). Classification and regression by randomForest. *R news*, 2(3), 18-22.

Littell, J. S., Mckenzie, D., Peterson, D. L., & Westerling, A. L. (2009). Climate and wildfire area burned in western U.S. ecoprovinces, 1916-2003. *Ecological Applications*, 19(4), 1003–1021. <https://doi.org/10.1890/07-1183.1>

Liu, X., Li, X., Chen, Y., Tan, Z., Li, S., & Ai, B. (2010). A new landscape index for quantifying urban expansion using multi-temporal remotely sensed data. *Landscape Ecology*, 25(5), 671–682. <https://doi.org/10.1007/s10980-010-9454-5>

Loehman, R. A. (2020). Drivers of wildfire carbon emissions. *Nature Climate Change*, 10(12), 1070–1071. <https://doi.org/10.1038/s41558-020-00922-6>

McCarley, T. R., Kolden, C. A., Vaillant, N. M., Hudak, A. T., Smith, A. M. S., Wing, B. M., Kellogg, B. S., & Kreitler, J. (2017). Multi-temporal LiDAR and Landsat quantification of fire-induced changes to forest structure. *Remote Sensing of Environment*, 191, 419–432. <https://doi.org/10.1016/j.rse.2016.12.022>

Miller, J. D., Knapp, E. E., Key, C. H., Skinner, C. N., Isbell, C. J., Creasy, R. M., & Sherlock, J. W. (2009). Calibration and validation of the relative differenced Normalized Burn Ratio (RdNBR) to three measures of fire severity in the Sierra Nevada and Klamath Mountains, California, USA. *Remote Sensing of Environment*, 113(3), 645–656. <https://doi.org/10.1016/j.rse.2008.11.009>

- Miller, J. D., Skinner, C. N., Safford, H. D., Knapp, E. E., & Ramirez, C. M. (2012). Trends and causes of severity, size, and number of fires in northwestern California, USA. *Ecological Applications*, 22(1), 184–203. <https://doi.org/10.1890/10-2108.1>
- Miller, J. D., & Thode, A. E. (2007). Quantifying burn severity in a heterogeneous landscape with a relative version of the delta Normalized Burn Ratio (dNBR). *Remote Sensing of Environment*, 109(1), 66–80. <https://doi.org/10.1016/j.rse.2006.12.006>
- Morgan, P., Heyerdahl, E. K., & Gibson, C. E. (2008). Multi-season climate synchronized forest fires throughout the 20th century, northern Rockies, USA. *Ecology*, 89(3), 717–728. <https://doi.org/10.1890/06-2049.1>
- Muggeo, V. M. (2008). Segmented: an R package to fit regression models with broken-line relationships. *R news*, 8(1), 20-25.
- Negrón-Juárez, R. I., Chambers, J. Q., Marra, D. M., Ribeiro, G. H. P. M., Rifai, S. W., Higuchi, N., & Roberts, D. (2011). Detection of subpixel treefall gaps with Landsat imagery in Central Amazon forests. *Remote Sensing of Environment*, 115(12), 3322–3328. <https://doi.org/10.1016/j.rse.2011.07.015>
- Obata, S., Cieszewski, C. J., Lowe, R. C., & Bettinger, P. (2021). Random forest regression model for estimation of the growing stock volumes in georgia, usa, using dense landsat time series and fia dataset. *Remote Sensing*, 13(2), 1–18. <https://doi.org/10.3390/rs13020218>

- Olofsson, P., Foody, G. M., Herold, M., Stehman, S. V., Woodcock, C. E., & Wulder, M. A. (2014). Good practices for estimating area and assessing accuracy of land change. *Remote Sensing of Environment*, 148, 42–57. <https://doi.org/10.1016/j.rse.2014.02.015>
- Omernik, J. M., & Griffith, G. E. (2014). Ecoregions of the Conterminous United States: Evolution of a Hierarchical Spatial Framework. *Environmental Management*, 54(6), 1249–1266. <https://doi.org/10.1007/s00267-014-0364-1>
- Owen, S. M., Sieg, C. H., Sánchez Meador, A. J., Fulé, P. Z., Iniguez, J. M., Baggett, L. S., Fornwalt, P. J., & Battaglia, M. A. (2017). Spatial patterns of ponderosa pine regeneration in high-severity burn patches. *Forest Ecology and Management*, 405, 134–149. <https://doi.org/10.1016/j.foreco.2017.09.005>
- Parks, S. A., & Abatzoglou, J. T. (2020). Warmer and drier fire seasons contribute to increases in area burned at high severity in Western US Forests from 1985 to 2017. *Geophysical Research Letters*, 47(22). <https://doi.org/10.1029/2020GL089858>
- Parks, S. A., Dobrowski, S. Z., Shaw, J. D., & Miller, C. (2019). Living on the edge: trailing edge forests at risk of fire-facilitated conversion to non-forest. *Ecosphere*, 10(3). <https://doi.org/10.1002/ecs2.2651>
- Parks, S. A., Holsinger, L. M., Panunto, M. H., Jolly, W. M., Dobrowski, S. Z., & Dillon, G. K. (2018). High-severity fire: Evaluating its key drivers and mapping its probability across western US forests. *Environmental Research Letters*, 13(4). <https://doi.org/10.1088/1748-9326/aab791>

Parks, S. A., Holsinger, L. M., Voss, M. A., Loehman, R. A., & Robinson, N. P. (2018). Mean composite fire severity metrics computed with google earth engine offer improved accuracy and expanded mapping potential. *Remote Sensing*, 10(6).

<https://doi.org/10.3390/rs10060879>

Pelletier, F., Eskelson, B. N. I., Monleon, V. J., & Tseng, Y. C. (2021). Using landsat imagery to assess burn severity of national forest inventory plots. *Remote Sensing*, 13(10).

<https://doi.org/10.3390/rs13101935>

Picotte, J. J., Peterson, B., Meier, G., & Howard, S. M. (2016). 1984-2010 trends in fire burn severity and area for the conterminous US. *International Journal of Wildland Fire*, 25(4),

413–420. <https://doi.org/10.1071/WF15039>

R Core Team. (2021). R: A language and environment for statistical computing. *R Foundation for Statistical Computing, Vienna, Austria*.

Riley, K. L., & Loehman, R. A. (2016). Mid-21st century climate changes increase predicted fire occurrence and fire season length, Northern Rocky Mountains, United States. *Ecosphere*,

7(11). <https://doi.org/10.1002/ecs2.1543>

Ruefenacht, B., Finco, M., Czaplewski, R., Helmer, E., Blackard, J., Holden, G., Lister, A., Salajanu, D., Weyermann, D., & Winterberger, K. (2008). Conterminous U.S. and Alaska Forest Type Mapping Using Forest Inventory and Analysis Data.

- Russell, R. E., Saab, V. A., Dudley, J. G., & Rotella, J. J. (2006). Snag longevity in relation to wildfire and postfire salvage logging. *Forest Ecology and Management*, 232(1–3), 179–187. <https://doi.org/10.1016/j.foreco.2006.05.068>
- Sankey, T., & Glenn, N. (2011). Landsat-5 TM and lidar fusion for sub-pixel juniper tree cover estimates in a Western Rangeland. *Photogrammetric Engineering and Remote Sensing*, 77(12), 1241. <https://doi.org/10.14358/PERS.77.12.1241>
- Schoennagel, T., Smithwick, E. A. H., & Turner, M. G. (2008). Landscape heterogeneity following large fires: Insights from Yellowstone National Park, USA. *International Journal of Wildland Fire*, 17(6), 742–753. <https://doi.org/10.1071/WF07146>
- Schoennagel, T., Veblen, T. T., & Romme, W. H. (2004). The interaction of fire, fuels, and climate across Rocky Mountain forests. *BioScience*, 54(7), 661–676. [https://doi.org/10.1641/0006-3568\(2004\)054\[0661:TIOFFA\]2.0.CO](https://doi.org/10.1641/0006-3568(2004)054[0661:TIOFFA]2.0.CO)
- Sellers, P. J. (1985). Canopy reflectance, photosynthesis and transpiration. *International Journal of Remote Sensing*, 6(8), 1335–1372. <https://doi.org/10.1080/01431168508948283>
- Shakesby, R. A., & Doerr, S. H. (2006). Wildfire as a hydrological and geomorphological agent. *Earth-Science Reviews*, 74(3–4), 269–307. <https://doi.org/10.1016/j.earscirev.2005.10.006>
- Sommers, W. T., Loehman, R. A., & Hardy, C. C. (2014). Wildland fire emissions, carbon, and climate: Science overview and knowledge needs. *Forest Ecology and Management*, 317, 1–8. <https://doi.org/10.1016/j.foreco.2013.12.014>

- Song, C., Schroeder, T. A., & Cohen, W. B. (2007). Predicting temperate conifer forest successional stage distributions with multitemporal Landsat Thematic Mapper imagery. *Remote Sensing of Environment*, *106*(2), 228–237.
<https://doi.org/10.1016/j.rse.2006.08.008>
- Sparks, A. M., Boschetti, L., Tinkham, W. T., Smith, A. M. S., Lannom, K. O., & Newingham, B. A. (2014). An accuracy assessment of the MTBS burned area product for shrub-steppe fires in the northern Great Basin, United States. *International Journal of Wildland Fire*.
<https://doi.org/10.1071/wf13206>
- Steel, Z. L., Fogg, A. M., Burnett, R., Roberts, L. J., & Safford, H. D. (2022). When bigger isn't better—Implications of large high-severity wildfire patches for avian diversity and community composition. *Diversity and Distributions*, *28*(3), 439–453.
<https://doi.org/10.1111/ddi.13281>
- Stevens, J. T., Lydersen, J. M., & Collins, B. M. (2018). Postfire restoration framework for national forests in California Appendix 4: Burn severity spatial analyses. In *General Technical Report: Vol. PSW-GTR-270* (pp. 175–182).
- Stevens-Rumann, C. S., Kemp, K. B., Higuera, P. E., Harvey, B. J., Rother, M. T., Donato, D. C., Morgan, P., & Veblen, T. T. (2018). Evidence for declining forest resilience to wildfires under climate change. *Ecology Letters*, *21*(2), 243–252. <https://doi.org/10.1111/ele.12889>
- Stevens-Rumann, C. S., & Morgan, P. (2016). Repeated wildfires alter forest recovery of mixed-conifer ecosystems. *Ecological Applications*, *26*(6), 1842–1853.
<https://doi.org/10.1890/15-1521.1>

- Szpakowski, D. M., & Jensen, J. L. R. (2019). A review of the applications of remote sensing in fire ecology. *Remote Sensing*, 11(22). <https://doi.org/10.3390/rs11222638>
- Thapa, B., Wolter, P. T., Sturtevant, B. R., & Townsend, P. A. (2020). Reconstructing past forest composition and abundance by using archived Landsat and national forest inventory data. *International Journal of Remote Sensing*, 41(10), 4022–4056. <https://doi.org/10.1080/01431161.2019.1711245>
- Thomas, D., Butry, D., Gilbert, S., Webb, D., & Fung, J. (2017). The costs and losses of wildfires: A literature survey (NIST Special Publication 1215). <https://doi.org/10.6028/NIST.SP.1215>
- Tinkham, W. T., Mahoney, P. R., Hudak, A. T., Domke, G. M., Falkowski, M. J., Woodall, C. W., & Smith, A. M. (2018). Applications of the United States Forest Inventory and Analysis dataset: a review and future directions. *Canadian Journal of Forest Research*, 48(11), 1251-1268. <https://doi.org/10.1139/cjfr-2018-0196>
- Townsend, P. A., & Walsh, S. J. (2001). Remote sensing of forested wetlands: application of multitemporal and multispectral satellite imagery to determine plant community composition and structure in southeastern USA. *Plant Ecology*, 157, 129-149.
- Trenberth, K. E., Branstator, G. W., & Arkin, P. A. (1988). Origins of the 1988 North American drought. *Science*, 242(4886), 1640-1645.
- Tucker, C. J. (1979). Red and Photographic Infrared Linear Combinations for Monitoring Vegetation. *Remote Sensing of the Environment*, 8, 127–150. [https://doi.org/10.1016/0034-4257\(79\)90013-0](https://doi.org/10.1016/0034-4257(79)90013-0)

- Turner, M. G., Braziunas, K. H., Hansen, W. D., & Harvey, B. J. (2019). Short-interval severe fire erodes the resilience of subalpine lodgepole pine forests. *Proceedings of the National Academy of Sciences of the United States of America*, *166*(23), 11319–11328.
<https://doi.org/10.1073/pnas.1902841116>
- Turner, M. G., Romme, W. H., & Gardner, R. H. (1999). Prefire heterogeneity, fire severity, and early postfire plant reestablishment in subalpine forests of Yellowstone National Park, Wyoming. *International Journal of Wildland Fire*, *9*(1), 21–36.
<https://doi.org/10.1071/wf99003>
- Vanderhoof, M. K., & Hawbaker, T. J. (2018). It matters when you measure it: Using snow-cover Normalised Difference Vegetation Index (NDVI) to isolate post-fire conifer regeneration. *International Journal of Wildland Fire*, *27*(12), 815–830. <https://doi.org/10.1071/WF18075>
- Vanderhoof, M. K., Hawbaker, T. J., Ku, A., Merriam, K., Berryman, E., & Cattau, M. (2021). Tracking rates of postfire conifer regeneration vs. deciduous vegetation recovery across the western United States. *Ecological Applications*, *31*(2).
<https://doi.org/10.1002/eap.2237>
- Viana-Soto, A., García, M., Aguado, I., & Salas, J. (2022). Assessing post-fire forest structure recovery by combining LiDAR data and Landsat time series in Mediterranean pine forests. *International Journal of Applied Earth Observation and Geoinformation*, *108*.
<https://doi.org/10.1016/j.jag.2022.102754>

- Vukomanovic, J., & Steelman, T. (2019). A Systematic Review of Relationships Between Mountain Wildfire and Ecosystem Services. *Landscape Ecology*, *34*(5), 1179–1194. <https://doi.org/10.1007/s10980-019-00832-9>
- Wang, C., Wang, A., Guo, D., Li, H., & Zang, S. (2022). Off-peak NDVI correction to reconstruct Landsat time series for post-fire recovery in high-latitude forests. *International Journal of Applied Earth Observation and Geoinformation*, *107*. <https://doi.org/10.1016/j.jag.2022.102704>
- Wang, X. Y., Wang, J., Jiang, Z. Y., Li, H. Y., & Hao, X. H. (2015). An effective method for snow-cover mapping of dense coniferous forests in the upper Heihe River Basin using Landsat Operational Land Imager data. *Remote Sensing*, *7*(12), 17246–17257. <https://doi.org/10.3390/rs71215882>
- Westerling, A. L., Hidalgo, H. G., Cayan, D. R., & Swetnam, L. W. (2006). Warming and earlier spring increase Western U.S. forest wildfire activity. *Science*, *313*(5789), 940–943. <https://doi.org/10.1126/science.1128834>
- Westerling, A. L., Turner, M. G., Smithwick, E. A. H., Romme, W. H., & Ryan, M. G. (2011). Continued warming could transform greater yellowstone fire regimes by mid-21st century. *Proceedings of the National Academy of Sciences of the United States of America*, *108*(32), 13165–13170. <https://doi.org/10.1073/pnas.1110199108>
- White, J. C., Saarinen, N., Kankare, V., Wulder, M. A., Hermosilla, T., Coops, N. C., Pickell, P. D., Holopainen, M., Hyyppä, J., & Vastaranta, M. (2018). Confirmation of post-harvest spectral recovery from Landsat time series using measures of forest cover and height derived from

airborne laser scanning data. *Remote Sensing of Environment*, 216, 262–275.

<https://doi.org/10.1016/j.rse.2018.07.004>

White, J. C., Wulder, M. A., Hermosilla, T., Coops, N. C., & Hobart, G. W. (2017). A nationwide annual characterization of 25 years of forest disturbance and recovery for Canada using Landsat time series. *Remote Sensing of Environment*, 194, 303–321.

<https://doi.org/10.1016/j.rse.2017.03.035>

White, J. D., Ryan, K. C., Key, C. C., & Running, S. W. (1996). Remote sensing of forest fire severity and vegetation recovery. *Int. J. Wildland Fire*, 6(3), 125–136.

<https://doi.org/10.1071/WF9960125>

Williams, A. P., & Raymond, E. (2002). Estimation of leafy spurge cover from hyperspectral imagery using mixture tuned matched filtering. *Remote Sensing of Environment*, 82, 446–456. [https://doi.org/10.1016/S0034-4257\(02\)00061-5](https://doi.org/10.1016/S0034-4257(02)00061-5)

Wolter, P. T., Mladenoff, D. J., Host, G. E., & Crow, T. R. (1995). Improved forest classification in the Northern Lake States using multi-temporal Landsat imagery. *Remote Sensing of Environment*, 210, 193–207.

Wolter, P. T., Townsend, P. A., Sturtevant, B. R., & Kingdon, C. C. (2008). Remote sensing of the distribution and abundance of host species for spruce budworm in Northern Minnesota and Ontario. *Remote Sensing of Environment*, 112(10), 3971–3982.

<https://doi.org/10.1016/j.rse.2008.07.005>

Wulder, M. A., White, J. C., Alvarez, F., Han, T., Rogan, J., & Hawkes, B. (2009). Characterizing boreal forest wildfire with multi-temporal Landsat and LIDAR data. *Remote Sensing of Environment*, 113(7), 1540–1555. <https://doi.org/10.1016/j.rse.2009.03.004>

Zhao, F. R., Meng, R., Huang, C., Zhao, M., Zhao, F. A., Gong, P., Yu, L., & Zhu, Z. (2016). Long-term post-disturbance forest recovery in the greater yellowstone ecosystem analyzed using Landsat time series stack. *Remote Sensing*, 8(11). <https://doi.org/10.3390/rs8110898>

Appendices

Appendix 1. List of the 34 high-severity wildfire events used in our analysis.

Fire ID	MTBS ID	MTBS Name	Year	Ecoregion	Dominant Conifer Forest Type	Area (acres)	High Severity %
Fire_1_1988	WY4463411003119880709 WY4473710995419880709 WY4491210990219880711	MIST CLOVERMIST CLOVER	1988	Middle Rockies	Fir-spruce	342,005	27.3%
Fire_2_1988	MT4507511010219880619 WY4499211096519880625 WY4470811082119880722 WY4509511033019880815	STORM CREEK FAN NORTH FORK HELLROARING	1988	Middle Rockies	Lodgepole pine	777,690	27.6%
Fire_3_1988	WY4422111042119880623 WY4438611053919880623 WY4434411052419880623 WY4430211056619880701 WY4412411002019880711 WY4419311073119880712 WY4408111047019880820	SNAKE SHOSHONE REDSHONE COMPLEX RED MINK FALLS HUCK	1988	Middle Rockies	Lodgepole pine	448,911	21.1%
Fire_4_1988	MT4605911433119880722 MT4604211426919880906	ROCK CREEK LITTLE ROCK CREEK	1988	Idaho Batholith	Douglas-fir	5,651	16.1%
Fire_7_1988	MT4724011275119880625	CANYON CREEK	1988	Middle Rockies	Lodgepole pine	167,870	50.4%
Fire_9_1988	ID4482611469819880705	MCCARTE RIDGE	1988	Idaho Batholith	Douglas-fir	8,312	16.7%
Fire_10_1988	MT4781311293519880711	GATES PARK	1988	Canadian Rockies	Lodgepole pine	42,492	52.5%
Fire_11_1988	ID4527011497119880711	SLIVER CREEK	1988	Idaho Batholith	Fir-spruce	45,075	42.7%

Fire ID	MTBS ID	MTBS Name	Year	Ecoregion	Dominant Conifer Forest Type	Area (acres)	High Severity %
Fire_12_1988	MT4795610858219880722	MONUMENT	1988	Middle Rockies	Lodgepole pine	5,633	24.1%
Fire_13_1988	ID4409711540519880726	WILLIS GULCH	1988	Idaho Batholith	Douglas-fir	4,962	24.8%
Fire_14_1988	MT4643911179319880809	CANYON CREEK	1988	Middle Rockies	Douglas-fir	35,864	46.5%
Fire_15_1988	ID4612911474719880811	FREEMAN TRAIL	1988	Idaho Batholith	Fir-spruce	19,499	28.5%
Fire_16_1988	MT4609711438119880814	SOUTH LOST HORSE	1988	Idaho Batholith	Fir-spruce	5,626	9.1%
Fire_18_1988	WY4431210701519880814	LOST	1988	Middle Rockies	Lodgepole pine	13,108	48.0%
Fire_19_1988	MT4612811450619880816	UPPER BEAR	1988	Idaho Batholith	Fir-spruce	7,241	26.7%
Fire_20_1988	MT4635311433619880817	TOTEM PEAK	1988	Idaho Batholith	Fir-spruce	6,559	12.8%
Fire_22_1988	WY4291010958419880821	FAYETTE	1988	Middle Rockies	Lodgepole pine	29,233	16.0%
Fire_23_1988	MT4701411039419880824	IRON CLAIM	1988	Middle Rockies	Douglas-fir	1,363	41.0%
Fire_25_1988	WA4843511857519880825	S.17MILE1	1988	Northern Rockies	Douglas-fir	8,089	25.4%
Fire_26_1988	MT4643311337819880825	COMBINATION	1988	Middle Rockies	Douglas-fir	8,588	56.0%
Fire_28_1988	WA4855511850019880825	WHITE MOUNTAIN	1988	Northern Rockies	Douglas-fir	21,854	25.1%
Fire_29_1988	MT4878711426219880906	RED BENCH	1988	Canadian Rockies	Douglas-fir	33,844	26.5%

Fire ID	MTBS ID	MTBS Name	Year	Ecoregion	Dominant Conifer Forest Type	Area (acres)	High Severity %
Fire_31_1988	ID4444911338919880907	LITTLE LOST	1988	Middle Rockies	Douglas-fir	6,282	46.9%
Fire_32_1989	ID4472811582819890726 ID4475711573919890726	NEEDLES SOUTH DOLLAR CREEK	1989	Idaho Batholith	Fir-spruce	13,334	15.2%
Fire_33_1989	WY4259410907119890704	ANNS	1989	Middle Rockies	Lodgepole pine	3,298	36.7%
Fire_35_1989	ID4409211552419890726	SMOKEY CREEK	1989	Idaho Batholith	Douglas-fir	47,680	2.4%
Fire_38_1989	ID4468911558619890726	LUNCH CREEK	1989	Idaho Batholith	Fir-spruce	7,443	28.5%
Fire_41_1989	ID4523011574819890726	STEAMBOAT	1989	Idaho Batholith	Fir-spruce	1,615	48.6%
Fire_42_1989	ID4472811552619890727	HORN CREEK	1989	Idaho Batholith	Lodgepole pine	2,488	33.3%
Fire_48_1990	MT4696611179819901113	BEARTOOTH COMPLEX	1990	Middle Rockies	Douglas-fir	13,461	18.8%
Fire_49_1991	MT4525511054919910716	THOMPSON CREEK	1991	Middle Rockies	Douglas-fir	6,978	31.2%
Fire_50_1991	ID4483111393719910825	MCKIM	1991	Middle Rockies	Douglas-fir	3,097	17.6%
Fire_51_1991	WY4361311022619911015	DRY COTTONWOOD	1991	Middle Rockies	Fir-spruce	6,995	13.5%
Fire_54_1991	MT4863211580519911016	UNNAMED	1991	Northern Rockies	Fir-spruce	2,478	51.2%

Appendix 2. Spectral indices used in conifer presence-absence Random Forest model creation.

Indices	Name	Equation	Purpose	Citation
NBR	Normalized Burn Ratio	$NBR = \frac{NIR - SWIR2}{NIR + SWIR2}$	Burn Severity	(García & Caselles, 1991)
RdNBR	Relativized Difference Normalized Burn Ratio	$\frac{NBR_{prefire} - NBR_{postfire}}{\sqrt{ NBR_{prefire} * 0.001 }}$	Burn Severity	(Miller & Thode, 2007)
NDVI	Normalized Difference Vegetation Index	$NDVI = \frac{NIR - RED}{NIR + RED}$	Vegetation	(Tucker, 1979)
EVI	Enhanced Vegetation Index	$EVI = 2.5 * \frac{NIR - RED}{NIR + 6 * RED - 7.5 * BLUE + 1}$	Vegetation	(Huete et al., 2002)
NDWI	Normalized Difference Water Index	$NDWI = \frac{GREEN - NIR}{GREEN + NIR}$	Moisture	(Gao, 1996)
NBR2	Normalized Burn Ratio 2	$NBR2 = \frac{SWIR1 - SWIR2}{SWIR1 + SWIR2}$	Burn Severity	(Key & Benson, 2006)
NDSI	Normalized Difference Snow Index	$NDSI = \frac{GREEN - SWIR1}{GREEN + SWIR1}$	Snow	(Hall & Riggs, 2010)
NDFSI	Normalized Difference Forest Snow Index	$NDFSI = \frac{NIR - SWIR1}{NIR + SWIR1}$	Snow	(Wang et al., 2015)